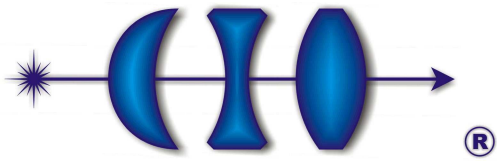

CENTRO DE INVESTIGACIONES
EN OPTICA, A.C.

SOLITON PROPAGATION IN HOLLOW-CORE PHOTONIC BANDGAP FIBERS: PULSE COMPRESSION AND SELF-FREQUENCY SHIFT

By

Noé González Baquedano

Submitted in partial fulfillment of the
requeriments for the degree of
DOCTOR IN SCIENCES (OPTICS)

PHOTONICS DIVISION,
CENTRO DE INVESTIGACIONES EN ÓPTICA, A.C.

LEÓN, GUANAJUATO, MÉXICO.

JUNE, 2013

Supervisors: Dr. Norberto Arzate Plata (CIO)
Dr. Ismael Torres Gómez (CIO)

Examiners: Dr. Alejandro Martínez Ríos (CIO)
Dr. Efraín Mejía Beltrán (CIO)
Dr. Daniel A. May Arrioja (Electronics Department, UAMRR, Autonomus University of Tamaulipas)

El temor de Jehová es el principio de la sabiduría
y el conocimiento del Santísimo es la inteligencia.

Salomón

A mi madre, hermanos
y a mi padre.

Table of contents

Table of contents iii

List of figures v

Abstract vii

Acknowledgements ix

1 Introduction 1
- 1.1 HC-PBGFs and their applications . . . 1
- 1.2 SPC and SSFS . . . 3
- 1.3 Scope of the thesis . . . 4

2 Modeling a HC-PBGF 7
- 2.1 Introduction . . . 7
- 2.2 Methodology . . . 10
- 2.3 Numerical results . . . 12
  - 2.3.1 Effective refractive index . . . 12
  - 2.3.2 Effective area and non linear parameter . . . 13
  - 2.3.3 Dispersion characteristics . . . 15
- 2.4 Conclusions . . . 18

3 Theory 19
- 3.1 Non linear pulse propagation . . . 19
  - 3.1.1 Solitons . . . 20
  - 3.1.2 Third-order dispersion . . . 23
  - 3.1.3 Intrapulse stimulated Raman scattering . . . 24
  - 3.1.4 TOD and ISRS . . . 25
- 3.2 Applications . . . 26

4 Results **29**
4.1 Modeled HC-PBGF 30
4.2 Soliton pulse compression 31
4.2.1 Influence of tuning the HC-PBGF 31
4.2.2 Pulse shape quality 35
4.2.3 Conclusions 41
4.3 Soliton self-frequency shift 42
4.3.1 Conclusions 54

5 Conclusions **57**

A Papers, conferences and workshops **61**

References **63**

List of Figures

1.1 First HC-PBGF 2

2.1 Studied HC-PBGF 9
2.2 Effective index of fundamental guided mode 12
2.3 Effective areas for air and silica 14
2.4 Non linear parameter for air and silica 15
2.5 Dispersion parameter as a function of tapering factor 16
2.6 Second- and third-order dispersion parameters 17

3.1 Evolution of a first order temporal soliton 21
3.2 Evolution of a third order temporal solitons 22
3.3 Spectral and temporal evolution of a third-order soliton with TOD . 23
3.4 Spectral and temporal evolution of a third-order soliton with ISRS . 25
3.5 Spectral and temporal evolution for a soliton with TOD and ISRS . 26

4.1 Seven-cell HC-PBGF and fundamental air-guided mode 30
4.2 Effective index for different tapering factors 31
4.3 Dispersion parameters for the studied fiber structures 32
4.4 Dispersion for the seven-cell HC-PBGF 33
4.5 Non linear parameter for the seven-cell HC-PBGF 34
4.6 Relative dispersion slope as a function of tapering factor 35

4.7 Pedestal energy evolution of the pulse as a function of tapering factor 36
4.8 Evolution of the FWHM and FC as a function of tapering factor . . 37
4.9 Pedestal energy vs FC of the seven-cell HC-PBGF 38
4.10 Output compressed pulses for different tapering factors of HC-PBGF 40
4.11 Optimum compressed pulse for a fiber with tapering factor of 4.5% . 41
4.12 Effective index for the A, B, and C studied fiber structures 42
4.13 Dispersion parameters for the A, B, and C studied fiber structures . 43
4.14 Non linear parameters for the A studied fiber structure 45
4.15 Relative dispersion slope for the A, B and C studied fiber structures 46
4.16 Density plots of the temporal and spectral evolution for a soliton, N=2 47
4.17 Compression factor as a function of length and soliton number . . . 48
4.18 Pulse quality factor as a function of length and soliton number . . . 49
4.19 Output compressed pulses for the A and B structures 50
4.20 Output compressed pulses for the C structure 51
4.21 Soliton self-frequency shift in the A and B fiber structures 53
4.22 Soliton self-frequency shift in the C fiber structure 54

Abstract

The purpose of this thesis is to investigate, by means of numerical simulations, soliton pulse compression and soliton self-frequency shift. Those physical phenomena are related to higher-order solitons propagation. This study in particular was performed in hollow-core photonic bangap fibers, and involves both designing and characterizing the fibers by means of their spatial parameters. A second stage consists in the study of soliton pulse propagation along the fiber and, as a consequence, the analysis of the desired phenomena. In particular, this work focus in the quality of the output pulse.

Firstly a brief introduction of hollow-core photonic bandgap fibers and theirs applications are shown: particularly soliton pulse compression and soliton self-frequency shift. Later a numerical investigation on the influence of tapering the fiber on its dispersion parameters, effective areas and non linear parameters are presented. Then the theoretical fundamentals for the study of soliton pulse propagation are given, as well as the mathematical expressions to quantify it.

Finally the soliton evolution is studied by solving the generalized Schrödinger equation. On the one hand, a numerical study of the compression of femtosecond unchirped pulses, at 800 nm is presented. Here the effects of tuning the cross section size of a HC-PBGF on the modal parameters in order to have a fiber structure which promotes pulse compression is studied. It was found that a tuning of the cross section

size of the fiber with a tapering factor of 4.5% produces a maximum compressed pulse with a compression factor of 5.7 with a temporal FWHM of 153.8 fs. The pulse reaches a peak power of 1.5851 MW with 77% of pulse shape quality. The length fiber at which the compressed pulse is reached is of 31 cm.

On the other hand, a numerical investigation of low-order soliton evolution at 1060 nm is presented. In the numerical simulation, the pulse quality evolution in soliton pulse compression and soliton self-frequency shift in three fiber structures with different cross-section sizes are investigated. The results showed that the seven-cell HC-PBGFs, with a cross section size reduction of 2%, presents larger anomalous values of the second-order dispersion and greater values of the non linear parameter. If an input soliton pulse with order of $N = 3$ (which corresponds to an energy of 1.69 μJ) propagates a distance of 12 cm, it gets compressed with a compression factor of 5.6 and quality factor of 0.73. Meanwhile, after the input soliton pulse propagates 6 m, its central wavelength redshifts to a shift value of $\Delta_\lambda = 28$ nm and presents a quality factor of ≈ 0.8.

Acknowledgements

- I want to thank my supervisors, Dr. Norberto Arzate Plata and Dr. Ismael Torres Gómez, for their help, patience and support during my doctoral studies. Without their help, this thesis could not have been accomplished.

- In the same way, I express my sincere gratitude to the reviewers: Dr. Efraín Mejía Beltrán, Dr. Alejandro Martínez Ríos and Dr. Daniel May Arrioja. Their comments, suggestions and corrections were of great help to improve the thesis.

- I would also like to thank Dr. Albert Ferrando Cogollos, from Universidad de Valencia, for giving me the opportunity to work with his group, during my predoctoral research visit, in the year 2010.

- I also appreciate and thank Dr. Pedro Fernández de Córdoba Castellá, from Universidad Politécnia de Valencia, for allow me to make use of the office and computing facilities of his group.

- In particular, I acknowledge the help and guidance of Dr. Daniel Ceballos and Dr. Carles Milián. And, above all, I acknowledge their friendship.

- To my friends Dr. José Luis Cabellos and M.Sc. Francisco Arteaga for all the talks regarding to the thesis work and some other topics which have motivated me to keep working during difficult times.

- I want to dedicate this thesis to my family, my parents Rosario Baquedano and Emerit González, as well as to my siblings, Efraín, Rebeca and Emerit. Their motivation, support and comprehension were of vital importance for me to conclude my doctoral studies. I would also like to dedicate this thesis to Mayalin Flores. Maya: "gracias por tu paciencia, comprensión y amor, has hecho mi vida más dulce, te amo princesa".

- I acknowledge the facilities and support of the Centro de Investigaciones en Óptica, A. C.

- I acknowledge the economic support of Consejo Nacional de Ciencia y Tecnología under scholarship number 207939. I also acknowledge partial support under the research grant 106764 (CB-2008-1).

- Finally, I thank God for His help during all this time.

1 Introduction

The main subject of the present thesis is to investigate, by means of numerical simulations, the following non linear phenomena: soliton pulse compression (SPC) and soliton self-frequency shift (SSFS) for hollow-core photonic bandgap fibers (HC-PBGFs). Such non linear optical phenomena have several applications on the temporal compression and the displacement of the central wavelength of an initial soliton pulse. HC-PBGFs were choosen as the non linear media due to their special characteristics of waveguiding and non linear properties [1].

1.1 HC-PBGFs and their applications

The HC-PBGF was first proposed by Russel in 1991 [2], theoretically demostrated by Birks in 1995 [3], and then experimentally proved by Cregan et al. in 1999 [4] (see Figure 1.1). Such a fiber had a triangular lattice of air holes in a silica background and the hollow core was formed by removing seven capillaries. The HC-PBGFs are characterized by a core with a lower refractive index compared with that of the cladding. Thus total internal reflection cannot occur, instead the light is guided and confined in the core, through Bragg reflection, by the surrounding photonic structure that is formed by a two-dimensional periodic array of air holes.

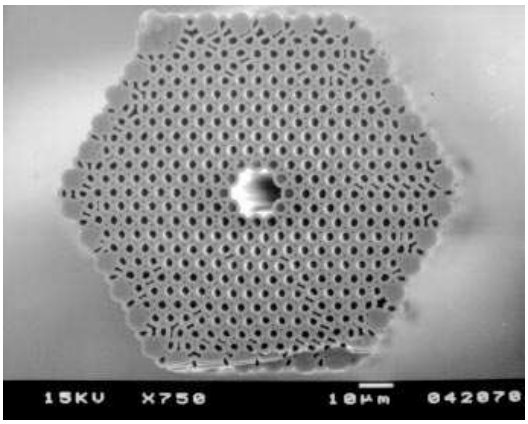

Figure 1.1: First hollow-core photonic bandgap fiber made by Cregan and his group [4].

It has been more than a decade since the first desing of HC-PBGF was made, and in all recent years, there has been a great progress in design, material and guidance capabilities of these kind of fibers [5, 6, 7, 8, 9]. For example, HC-PBGFs with triangular, square, and kagome lattices are now possible to fabricate. The scientific community is making great efforts in order to achieve hollow fibers with larger transmission bands, with low losses and better guiding features by probing novel geometry desings of both the core and the surrounding structure, and as well as the material that forms the fiber. Simultaneously, they are also looking for potential applications which include: optical gyroscopes, industrial applications, sensing, high-power pulse transmision, gas cell, pulse compression, etc. Among the advantages of HC-PBGFs based optical gyroscopes over solid core fibers are: low non linearities, pure silica material, no Fresnel reflections, polarization maintaining desing and low bend sensitivity [10, 11]. HC-PBGFs have also been used to deliver high-power CO_2 laser beams for industrial applications such as cutting, welding, and marking. By using HC-PBGFs, researchers overcome the problem of

utilizing a bulky system to bring high-power beams from the source to the working area [12, 13, 14, 15]. Sensing is another field in which HC-PBGFs have found a niche. The motivation is thay they can offer better features than solid-core fibers. Applications of interest include environmental sensing, process monitoring, biosensing, gas sensing, etc [16, 17, 18, 19, 20, 21, 22, 23]. Besides, HC-PBGFs have been designed for the transmission of high-peak-power ultra-short laser pulses [24, 25] and present themselves as an attractive option for laser dentistry and biomedical applications [26, 27, 28]. Another interesting feature of HC-PBGFs is their capacity for being used as gas cells [29, 30, 31]. Some novel results have already been demonstrated in areas such as non linear optics [32, 33, 34, 35, 36, 37, 38], quantum optics [39, 40] laser-induced guidance [41], etc.

1.2 SPC and SSFS

Two non linear phenomena that might take place during the propagation of pulses in optical fibers, and that are the subject of this thesis, are soliton pulse compression (SPC) and soliton self-frequency shift (SSFS). These phenomena are in continuous investigation by the scientific community [42, 43, 44, 45], and have an important role in the search of new technologies of light sources and applications based almost entirely on HC-PBGFs. Several research groups have made important advances both experimentally and theoretically in the understanding of soliton compression and soliton formation as well as its dynamics in HC-PBGFs [33, 46, 47]. Recently, in the study of SPC, Ouzounov et al. successfully compressed a 120 fs input pulse into 50 fs pulse by using a 24 cm Xe-filled HC-PBGF [43]. Gérôme et al. also reported the existence of soliton compression. They achieved output pulses of 90 fs from 195 fs input pulses by using 8 m of tapered fiber [44, 48]. Lægsgaard and Roberts studied numerically the soliton formation during the compression of chirped gaussian

pulses in HC-PBGFs. They concluded that third-order dispersion (TOD) is a crucial parameter that prevents the formation of shorter soliton pulses [49, 50]. Welch and collaborators demonstrated a temporal compression factor of 12, in a seven-cell hollow-core tapered fiber with a length of 35 m, for picosecond input pulses [51]. Meng et al. [45] numerically studied the soliton formation during the compression of unchirped femtosecond pulses in HC-PBGFs by using the Gorbach-Skryabin model [52]. They concluded that the combined effects of intrapulse stimulated Raman scattering and negative TOD can form shorter pulses than those formed by only considering intrapulse stimulated Raman scattering. Heckl et al. using a xenon gas-filled Kagome-type HC-PCF achieved a maximum compression factor of 4.3 and an efficiency of above 70% [53].

On the other hand, SSFS and their applications have also been studied [54, 55]. Ouzounov et al., for instance, reported a SSFS from 1470 nm to 1530 nm [33]. Making use of such phenomenon, Gérôme reported a high-power tunable femtosecond soliton source of 33 nm wavelength tunability [56]. Gorbach and Skryabin studied the dynamics that accompany the soliton propagation in the femtosecond regime in HC-PBGFs. Their model included non linear responses of both the silica, in the cladding, and of the air. They concluded that the strong Raman response of air does not always result in a large SSFS in HC-PBGFs [52].

1.3 Scope of the thesis

In the present thesis, soliton propagation in HC-PBGFs is studied. In particular, two non linear optical phenomena namely SPC and SSFS. Although SPC and SSFS have been studied by other authors, those studies lack of an analysis of the quality of the output pulse. Hence, in this work those phenomena are investigated under the

influence of variations of the characteristics of the fiber and the input soliton pulse. A conjoint analysis of the pulse shape quality in both phenomena, SPC and SSFS, is performed. According tho the author's best knowledge, this kind of analysis was first reported in [57], and here it is presented as the main scope of the thesis.

The outline of the thesis is as follows: chapter 2 presents a numerical investigation of the influence of tapering the cross section size of a seven-cell HC-PBGF on the dispersion, effective area and non linear parameters. Furthermore, this chapter presents some distinctive features that can help the reader to understand the main features of such kind of fibers. Although there are several geometries of HC-PBGFs, the simulated fiber, in this chapter, represents the most basic geometry: its cladding is formed by circular air-holes embedded in a triangular lattice of silica that surround the air-core. A detailed description of how to design or modelate HC-PBGFs is not the objective of this thesis. For a more comprehensive study of how to do so, the reader is refered to [58]. Therefore, the simulation only shows the behaviour of fundamental guided modes, which were used to find the refractive index of the air-guided modes. The Comsol Multiphysics, a powerfull commercial simulation software was used to find such air-guided fundamental modes*. This package was adapted to modelate HC-PBGFs. Once the refractive index was computed, a home-made Matlab code was used to find the dispersion and non linear parameters. The pulse propagation theory is then presented in Chapter 3. The generalized non linear Schrödinger equation (GNLSE) is used as a foundation to explain the soliton pulse propagation along the fiber. Definitions of the used mathematical model and the quantitative parameters as well as a brief explanation of the physical phenomena that involved the SPC and SSFS are given. Afterwards chapter 4 contains two numerical investigations of soliton propagation in HC-PBGFs. The first one

*I want to thank Dr. Albert Ferrando, from the Universidad de Valencia, for giving me the opportunity to work in his group and for letting me use COMSOL Multiphysics.

analyzes the enhancement of both the compression factor and the pulse shape quality of femtosecond pulses at the wavelength of 800 nm by tuning the cross section size of the fiber. The second one comprises a numerical study of low-order soliton evolution in a proposed seven-cell HC-PBGF. The numerical simulation analyzes the pulse quality evolution in soliton pulse compression and soliton self-frequency shift in three fiber structures with different cross section sizes at the wavelength of 1060 nm. In both works the Comsol Multiphysics software was used to model the HC-PBGF structures and the GNLSE was solved by using the symmetric split-step Fourier method. Finally, conclusions of the thesis are exposed in Chapter 5.

2 Modeling a HC-PBGF

A numerical study of the effects of tapering a hollow-core photonic bandgap fiber (HC-PBGF) on parameters such as effective area, non linear parameter and dispersion parameter is presented. The taper on the fiber is modeled by scaling the cross section of the original fiber geometry. Both the air and the silica contributions to the effective area and the non linear parameter are studied. Afterwards the fundamental guided mode and its respective effective refractive index for the HC-PBGFs are found. Once the effective refractive index of the mode is obtained, their corresponding dispersion and non linear parameters are computed. Since, a detailed description of how to design or modelate HC-PBGFs is not the objective of this thesis the simulation only shows the behavior of fundamental guided modes, which were used to find the refractive index of the air-guided modes. The Comsol Multiphysics, a powerfull commercial simulation software was used to find such air-guided fundamental modes. This package was adapted to modelate HC-PBGFs.

2.1 Introduction

The development of hollow-core photonic bandgap fibers meant a milestone in the study of non linear optical phenomena thanks to the special way in which light is guided: these allow us to confine light in a core of air, whose refractive index is lower

than that of the cladding [59, 60, 61]. In the case of air-filled HC-PCF, the effective nonlinearity is reduced by as much as three orders of magnitude when compared with solid-core fibers. But because the overall dispersion is generally anomalous over most of the transmission profile, guidance of high-peak-power pulses by means of non linear soliton effects is nonetheless possible [62].

Thus HC-PBGFs are an ideal medium for the delivery of light pulses of high intensity [43, 48]. Figure 2.1(a) shows the cross section of the HC-PBGF that is studied in this section. Basically, the fiber is made by an unique material (silica); the cladding is formed by air holes periodically located in a triangular arrangement, which extend along the length of the fiber, and surround the air core. The parameter d and the pitch, Λ, define the diameter of the air holes and the distance between consecutive holes, respectively. Another important parameter is D which represents the relative hole size that is defined by the ratio $D = d/\Lambda$. This parameter gives information about the quantity of silica that the fiber contains; a value of $D \geq 0.95$ indicates that the quantity of silica contained on the fiber is quite small.

Tapering conventional optical fibers is a well studied issue, both experimentally and theoretically. Thinning an optical fiber induces radical changes on the modal properties of the fiber [63]. HC-PBGFs already presents distinctive characteristics depending on both the geometry and the size of its structure (d and Λ). Thus the values of parameters such as the effective modal area (A_{eff}), the dispersion parameter ($\mathcal{D}$) [64], and the non linear parameter (γ) will change if the geometry and size of the fiber are changed. One way to incorporate an additional degree of freedom on the waveguiding properties of the fiber is to consider the tapering of the fiber [51]. Although the core of the fiber is made of air, the non linear parameter of the HC-PBGFs does not only arise from the contribution of the air, but also from the contribution of the silica. This is because part of the guided mode overlaps with

regions made of silica [65, 66]. Since the non linear refractive index of the silica is three orders of magnitude greater [67] than that of the air, it is interesting and important to compare both contributions to the non linear parameter.

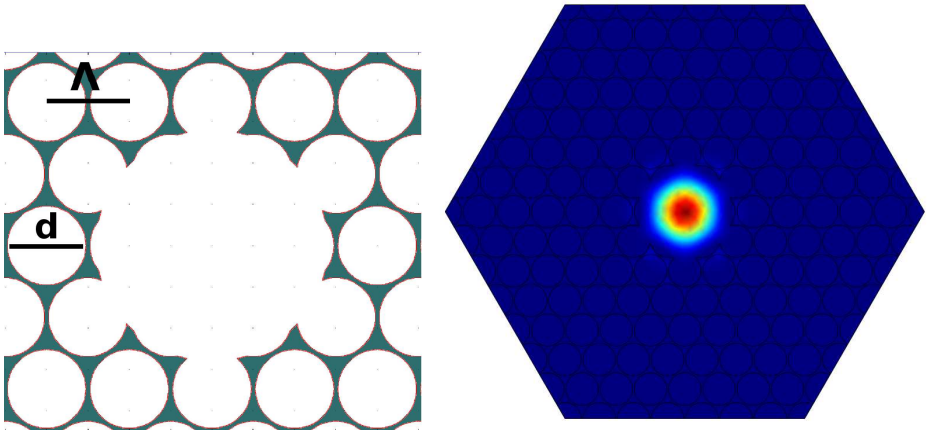

(a) (b)

Figure 2.1: (a) Cross section of the studied HC-PBGF. Λ and d represent the pitch and the diameter of the air hole, respectively. The colored region represents silica and the white region represents air. (b) Fundamental guided mode of the fiber shown in (a).

A remarkable characteristic of the HC-PBGFs is that the guided modes are only permitted for a range of wavelengths, which is directly related to the size of the bandgap of the cladding of the fiber (only light with wavelengths within the photonic bandgap of the cladding can be guided in the core). In other words, the transmission band width, the range of wavelengths of the light than can be guided along the core, is ruled by the size and geometry of the cladding of fiber [68]. Figure 2.1(b) shows a fundamental guided mode for the HC-PBGF that is depicted in Figure 2.1(a).

Among the non linear optical phenomena that can be studied in HC-PBGFs are the formation and dynamics of solitons along the fiber such as pulse compression and

self-frequency shift [49, 45]. The first step to evaluate such phenomena is to find the values of the spatial modal parameters of the fiber. The investigation considers that the fiber preserves its original form and geometry and only experiences a uniform decrease of its dimensions. It should be noticed that the tapering factor is not a function of the fiber length. Therefore the spatial parameters are not related to the length of the tapered fiber, but only with the cross secion size of the fiber.

2.2 Methodology

In order to find the effective refractive index of fundamental modes in a tapered HC-PBGF, the comercial software *Comsol Multyphysics*© is used. Furthermore the spatial parameters are also found: the modal effective area (for air and silica), the non linear parameter (for air and silica) and the dispersion parameter. The parameters of the untapered fiber structure are: $d = 1.9$ μm, $\Lambda = 2$ μm and $D = 0.95$. The tapered fiber is modeled by scaling the cross section of the original (untapered) structure of the HC-PBGF. Since the values of d and Λ are scaled by the same factor, the value of D is kept fixed. In this work, four sizes of the HC-PBGF are used. Those correspond to a fiber tapering factors of 0, 10, 20 and 30% of its original structure. Table 2.1 shows the particular values of d and Λ for each of these cases. The core of the fiber is composed by an air hole with a radius of $r = 1.4(\Lambda) = 2.8$ μm. The core of the fiber cuts six holes of the inner ring of the cladding as it is shown in Figure 2.1(a). The core's form of the HC-PBGF was chosen in such a way that it avoids surface modes [61].

The dispersion parameter takes into account the material dispersion and the waveguide dispersion, and it can be calculated by performing the second derivative of the effective index of a guided mode, n_{eff}, with respect to the wavelength, λ,

Table 2.1: Hole diameter, d, and pitch, Λ, values of the studied HC-PBGFs. $D = d/\Lambda$ is kept fixed with the value of $D = 0.95$.

Tapering factor (%)	d (μm)	Λ (μm)
0	1.9	2.0
10	1.71	1.8
20	1.52	1.6
30	1.33	1.4

as [69]:

$$\mathcal{D}(\lambda) = \left(\frac{\lambda}{c}\right)\left(\frac{\mathrm{d}^2 n_{eff}}{\mathrm{d}\lambda^2}\right), \tag{2.1}$$

where c is the velocity of light. We have calculated the effective area of fundamental guided modes for a HC-PBGF through the definition given by: [70]

$$A^i_{eff} = \frac{(\int_{-\infty}^{+\infty}\int_{-\infty}^{+\infty} \mid E \mid^2 \mathrm{d}x\mathrm{d}y)^2}{\int_{-\infty}^{+\infty}\int_{-\infty}^{+\infty} \mid E_i \mid^4 \mathrm{d}x\mathrm{d}y}, \quad i = a, s \tag{2.2}$$

where $i = a, s$ refers to air and silica, respectively; E is the electric field and thus E_i is the electric field either in the silica region or the air region. The above definition for A_{eff} is valid for low contrast fibers. This means that the effective refractive index of the fundamental guided mode must be approximately equal to the refractive index of the core, n_{core}, i.e., $n_{eff} \approx n_{core}$. Both contributions are shown, that of air and of silica, in order to see their contributions to the total non linear parameter, which is given by [67]:

$$\gamma_T = \gamma_a + \gamma_s, \tag{2.3}$$

with

$$\gamma_i = \frac{2\pi n_2^i}{\lambda A^i_{eff}}, \tag{2.4}$$

where n_2^i represents the non linear coefficient of the silica ($i = s$) or the air ($i = a$), and the A^i_{eff} is the effective area defined by Equation 2.2. The following values for

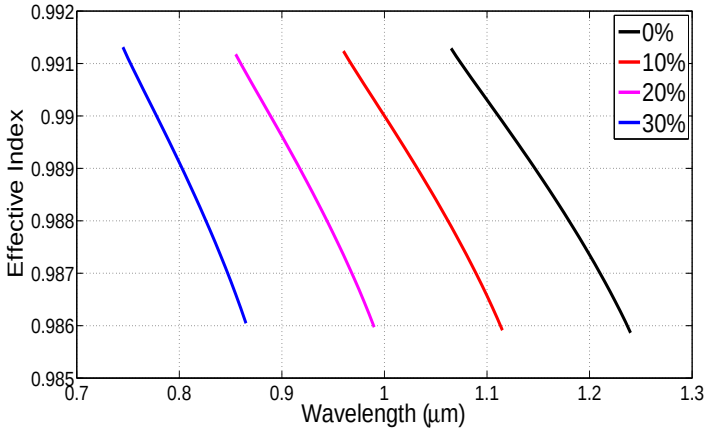

Figure 2.2: Computed effective refractive index of the fundamental guided modes as a function of wavelength, and fiber tapering factor.

the non linear coefficients are used: $n_2^a = 2.9 \times 10^{-23}$ m^2/W and $n_2^s = 2.6 \times 10^{-20}$ m^2/W [67]. All calculations for A_{eff} and γ_T performed correspond to fundamental guided modes.

2.3 Numerical results

2.3.1 Effective refractive index

The computed effective refractive index of the fundamental air-guided modes for the four HC-PBGFs as a function of the wavelength can be seen in Figure 2.2. For the original structure (with fiber tapering factor of 0 %), it can be observed that fundamental modes were found within the wavelength range of 1065 to 1240 nm. As long as the cross secion of the fiber gets reduced, the fundamental modes are found at lower wavelengths. For instance, for that fiber with a tapering of 30%, those modes are located within the wavelength range from 745 to 865 nm. Another

feature that is present in effective index curves of Figure 2.2 is their similar behavior, that can be understood by the symmetrically reduction of the cross secion size of the HC-PBGF.

These features play an important role since they give information about the needed tapering factor of the fiber in order to obtain air-guided modes within a given wavelength range.

2.3.2 Effective area and non linear parameter

Figure 2.3 shows the effective areas, for air and silica, of the fundamental guided mode of the HC-PBGF shown in Figure 2.1 for different values of fiber tapering factors. Since the core is made of air, let's mainly focus in its contribution. There are interesting features that we can address due to the tapering of the fiber: firstly, the transmission bandwidth of the untapered fiber is of around 175 nm. This value decreases as the tapering factor increases. This feature is clearly seen by observing that the transmission width is of around 120 nm for a tapering factor of 30%. The second feature is that the transmission band shifts to lower wavelengths as the tapering factor increases. From Figure 2.3(a), it can be seen that the transmission band is centered at around 1150 nm for the untapered fiber, and at around 800 nm for the fiber with a tapering factor of 30%. The third issue is a direct consequence of the thinning: if the diameter of the fiber's core decreases then the area in which the fundamental mode is confined also decreases and, therefore, its corresponding effective area decreases as well. The effective areas for both the air and the silica of the fundamental mode for an untapered fiber are nearly 2 times greater than those of the fiber with a tapering factor of 30%, at the wavelength of maximum effective area.

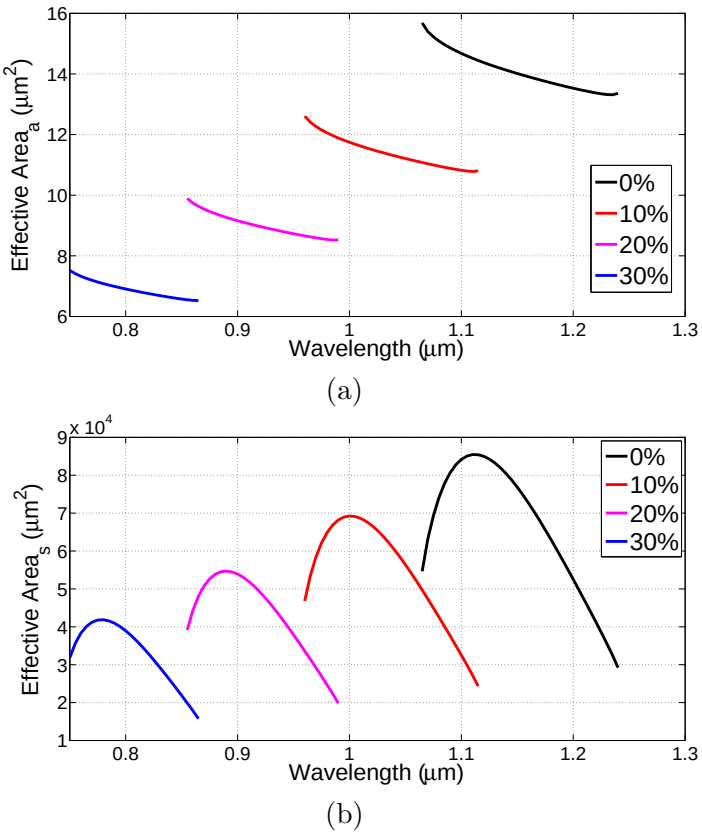

Figure 2.3: Effective areas for air (a) and silica (b) as a function of wavelength, and fiber tapering factor.

In regard to the non linear parameter curves, these are depicted in Figure 2.4. In a similar way, we can observe the following issues: a shift of the transmission band to lower wavelengths and an increase of the value of the non linear parameter as the tapering factor is increased. It can also be seen from Figure 2.4 that the non linear parameter due to the air contribution is greater than that of the silica and their difference increases as the tapering factor increases. For instance, the overall non linear parameter values due to the air contribution for the untapered fiber are of around 3 times lower than those of the tapered fiber with a tapering factor of 30%.

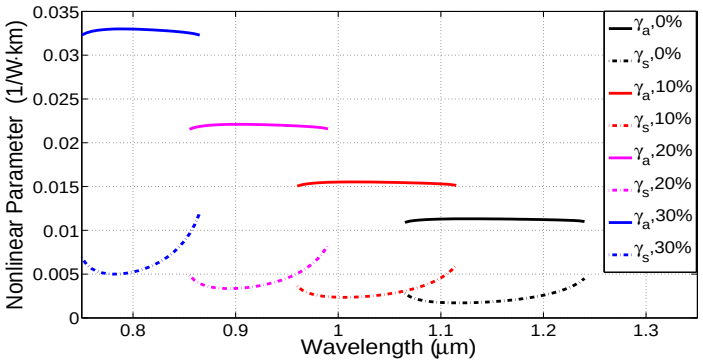

Figure 2.4: Computed non linear parameter of the fundamental guided modes of the studied HC-PBGF as a function of wavelength and fiber tapering factor. The solid and dotted curves correspond to the contributions of air and silica, respectively.

Besides the non linear parameter for air keeps almost constant in the wavelength range of the transmission band. This feature can be understood if we recall that only fundamental guided modes are considered. The changes that we expect in the effective area for air of those modes are small. Hence the variation of the non linear parameter for air is also small.

2.3.3 Dispersion characteristics

The dispersion parameter gives information about how much a light pulse is broadened per unit of length, and per unit of wavelength as it propagates along the fiber. Figure 2.5 shows the corresponding dispersion parameter for the studied HC-PBGF as a function of wavelength and tapering factor. It is observed from Figure 2.5 that as the tapering factor is increased, there is a shift of the dispersion curve to lower wavelengths. The calculated zero-dispersion wavelength (ZDW) for the untapered fiber is at around 1100 nm; as the tapering factor increases, the ZDW is blueshifted. For example, a fiber tapering factor of 10%, the ZDW is at around 980 nm, and with

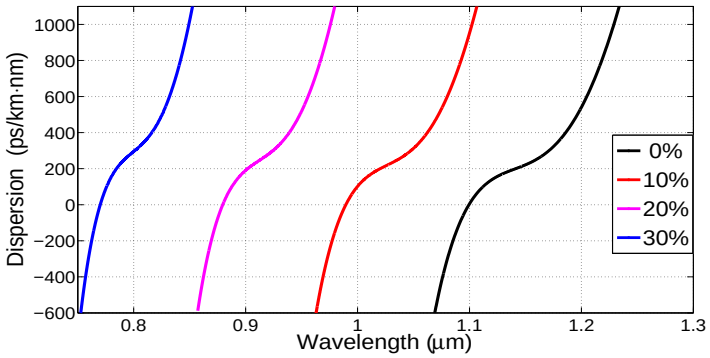

Figure 2.5: Computed dispersion parameter of the fundamental guided modes of the studied HC-PBGF as a function of wavelentgh and fiber tapering factor

a tapering factor of 30% we get a ZDW at around 780 nm. From Figure 2.5, we can also see that the values of the dispersion curve increase faster with wavelength as the tapering factor increases. Another feature that we can observe is the wavelength range where anomalous dispersion regime, $\mathcal{D} > 0$, takes place. As it was pointed out above, the transmission bandwidth of the untapered HC-PBGF is of around 175 nm; within this transmission wavelength range, anomalous dispersion takes place in a range of 145 nm. On the other hand, for the fiber with a tapering factor of 30%, the transmission bandwidth is of around 120 nm and within this range, the anomalous regime is present in a wavelength range of 100 nm. Thus the range of wavelength where anomalous dispersion takes place decreases for tapered fibers, compared to that of the untapered fiber. However, it is observed that the rate of the anomalous dispersion region to the transmission bandwidth is almost the same for all the fiber structures. For this particular geometry of HC-PBGF, the anomalous dispersion takes place in a percentage range of 83% of the total transmission bandwidth.

Second- (β_2) and third-order (β_3) dispersion parameters as a function of wavelength for the studied fiber structures are depicted in Figure 2.6. Most of the allowed

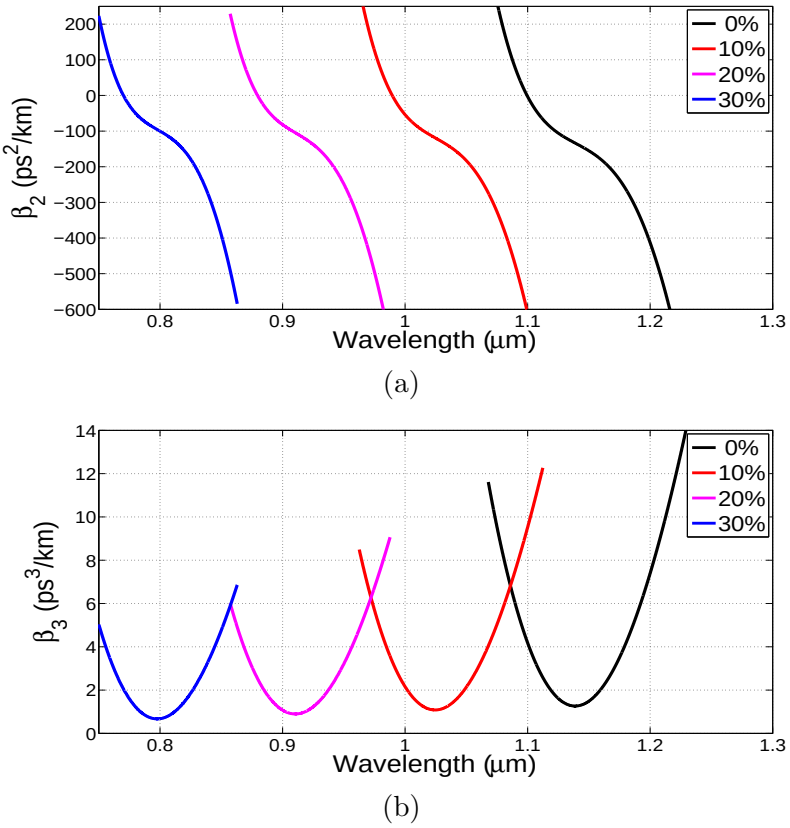

Figure 2.6: Second and third-order dispersion parameters as a function of wavelength, and fiber tapering factor.

wavelengths are in the anomalous region and, as expected, the effect of reducing the cross secion size of the HC-PBGF is the shift of the ZDW to shorter wavelengths, see Figure 2.6(a). With respect to the third-order dispersion parameter, their corresponding curves are shown in Figure 2.6(b). It can be noticed that all β_3 curves have positive values and their respective minima slightly decreases as the tapering factor increases.

2.4 Conclusions

A study of the effects that experience a HC-PBGF on its modal spatial parameters such as the effective area, the dispersion parameter and the non linear parameter due to a fiber tapering has been presented. The contributions of both the air and the silica to the non linear parameter and modal effective area were shown. From the results it was observed that the air contribution to the non linear parameter predominates. It was also shown that as the fiber tapering factor increases, the transmission band is blueshifted and its width decreases. Besides, the wavelength range where anomalous dispersion takes place is almost the same for different fiber tapering factors. On the other hand, the dispersion parameter curves blueshifts as the fiber tapering factor increases and their values increases faster with wavelength. The different features found on the effective area, the dispersion parameter and the non linear parameter have a great of importance on the design of fibers because, for example, they give information of the location of the ZDW, the wavelength range of the anomalous dispersion regime and the spectral behavior of the dispersion of the fiber. Thus the knowledge of the spectral behavior of the modal spatial parameters of the fundamental mode is quiet important in order to design and optimize a HC-PBGF that enhances a particular non linear optical effect.

3 Theory

In this chapter the equations that model the propagation of optical pulses in hollow-core photonic bandgap fibers (HC-PBGFs) are presented. The generalized non linear Schrödinger equation (GNLSE) is used to describe the optical pulse propagation, and is numerically solved in order to show the evolution of femtosecond pulses along the fiber. The behavior of higher-order solitons on its propagation through the fiber are depicted. In particular, the propagation of higher-order solitons is studied through the involved optical phenomena of soliton pulse compression (SPC) and soliton self-frequency shift (SSFS).

3.1 Non linear pulse propagation

Propagation pulses in fiber optics are ruled by the generalized non linear Schrödinger equation [52]:

$$\begin{aligned}\frac{\partial A}{\partial z} &= \sum_{k\geq 2}^{\infty} \frac{i^{k+1}}{k!}\beta_k \frac{\partial^k A}{\partial t^k} \\ &+i\gamma_a(1-f_a) \mid A \mid^2 A + i\gamma_a f_a A \int_{-\infty}^{+\infty} dt' R_a(t') \mid A(t-t',z) \mid^2 \\ &+i\gamma_s(1-f_s) \mid A \mid^2 A + i\gamma_s f_s A \int_{-\infty}^{+\infty} dt' R_s(t') \mid A(t-t',z) \mid^2, \quad (3.1)\end{aligned}$$

where $A = A(t, z)$ is the slowly-varying pulse envelope in a co-moving frame, t is the time, and z is the spatial coordinate along the fiber. The corresponding contributions to the Raman response function due to air, R_a, and silica, R_s, are described by [71]:

$$R_i(t) = \Theta(t)\frac{(\tau_1^{(i)})^2 + (\tau_2^{(i)})^2}{\tau_1^{(i)}(\tau_2^{(i)})^2} \exp\left[-t/\tau_2^{(i)}\right] \sin\left(t/\tau_1^{(i)}\right), \tag{3.2}$$

where $\Theta(t)$ is the Heaviside function, τ_1 and τ_2 are the Raman parameters, which values for silica are well known and have the following values [71]: $\tau_1^s = 12.2\,\text{fs}$, $\tau_2^s = 32\,\text{fs}$ and $f_s = 0.18$. Meanwhile, the estimated values for air are [52]: $\tau_1^a = 62\,\text{fs}$, $\tau_2^a = 77\,\text{fs}$ and $f_a = 0.5$. The dispersion parameters, β_k, can be computed expanding the propagation constant, $\beta(\omega)$, around the central frequency ω_0 as [71]

$$\beta(\omega) = \beta(\omega_0) + \beta_1(\omega_0)\Omega + (1/2)\beta_2(\omega_0)\Omega^2 + (1/6)\beta_3(\omega_0)\Omega^3 + ..., \tag{3.3}$$

where $\Omega = \omega - \omega_0$, and

$$\beta_k(\omega_0) = \left.\frac{d^k\beta}{d\omega^k}\right|_{\omega_0}. \tag{3.4}$$

Losses are neglected due to the short length of the fibers. Furthermore effects such as self-steepening, two-photon absorption and plasma generation have also been neglected in the model because it is assumed that the described spectral evolution takes place away from the zero group-velocity dispersion, GVD, wherein such phenomena are no significant [52].

3.1.1 Solitons

Temporal solitons in fiber optics are formed due to a balance between the GVD and the selph-phase modulation, SPM [72], and are ruled by the equation:

$$\frac{\partial A}{\partial z} + \frac{i}{2}\beta_2\frac{\partial^2 A}{\partial t^2} = i(\gamma_a + \gamma_s) \mid A \mid^2 A. \tag{3.5}$$

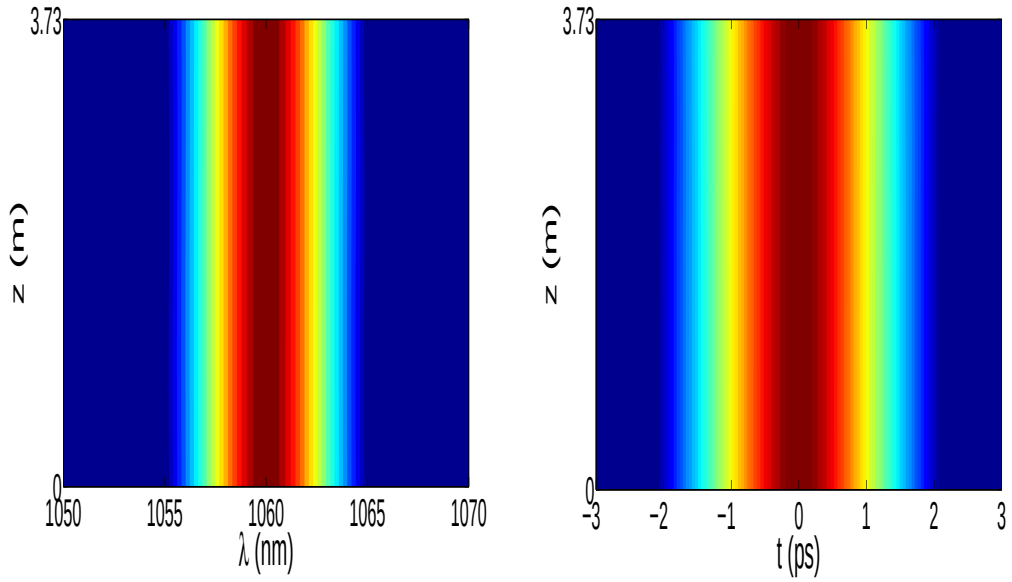

Figure 3.1: Spectral and temporal evolution of a first-order temporal soliton over one soliton period.

If we consider an input pulse of the form:

$$A(0,t) = N \,\mathrm{sech}\,(t/t_0), \tag{3.6}$$

the pulse remains unchanged as it propagates along the fiber for $N = 1$ (see Figure 3.1), and presents a periodic behavior for integers values of $N > 1$ in such a way that the initial pulse shape is recovered after a certain distance (see Figure 3.2). The parameter N defines the soliton order and contains information about both the optical fiber and the input pulse and is given by [73]:

$$N^2 = \gamma_T P_0 L_D = (t_0^2 \gamma_T P_0)/|\beta_2|, \tag{3.7}$$

where L_D is the dispersion lenght, P_0 and t_0 are the peak power and width of the initial pulse, respectively.

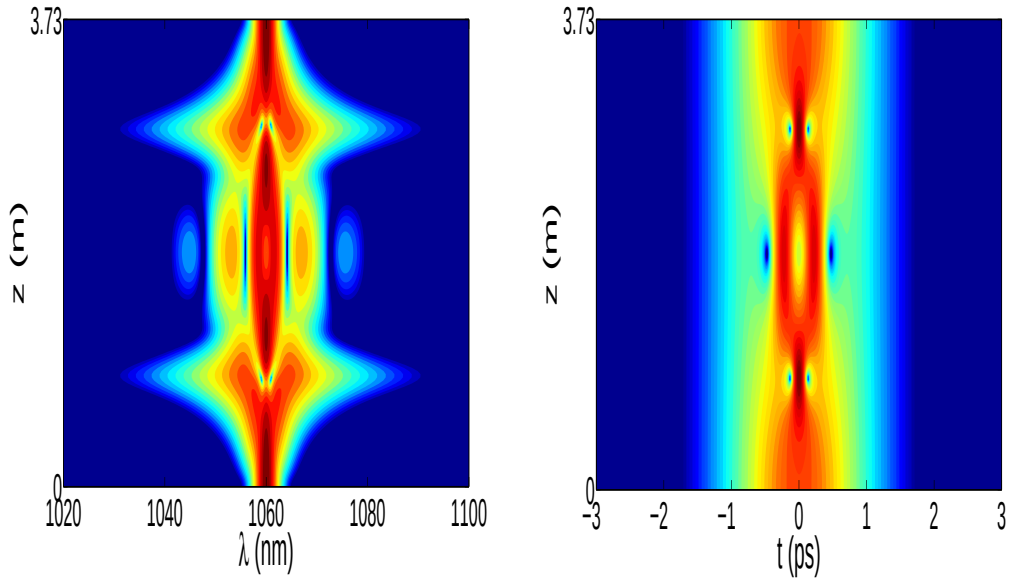

Figure 3.2: Spectral evolution of a third-order temporal soliton over one soliton period.

Hence for $N = 1$, a fundamental soliton is formed and, for $N > 1$, higher-order solitons are generated. The soliton period is defined as the distance over which higher-order solitons recover their original shape and is given by:

$$z_{sol} = \frac{\pi}{2} L_D = \frac{\pi}{2} \frac{t_0^2}{|\beta_2|}. \tag{3.8}$$

Given the HC-PBGF parameters: $\beta_2 = -67$ ps^2/km, $\gamma_a = 7.702 \times 10^{-3}(\text{W} \cdot \text{km})^{-1}$, $\gamma_s = 2.978 \times 10^{-3}(\text{W} \cdot \text{km})^{-1}$; and the input pulse characteristics: $t_0 = 400$ fs and $P_0 = 39.323$ kW. It gets $N = 1$. From Figure 3.1, it can be seen the spectral and temporal evolution of a fundamental soliton as it propagates along the fiber. As it was mentioned above, the fundamental soliton does not change with propagation.

Increasing the peak power to $P_0 = 360$ kW but keeping all the others parameters

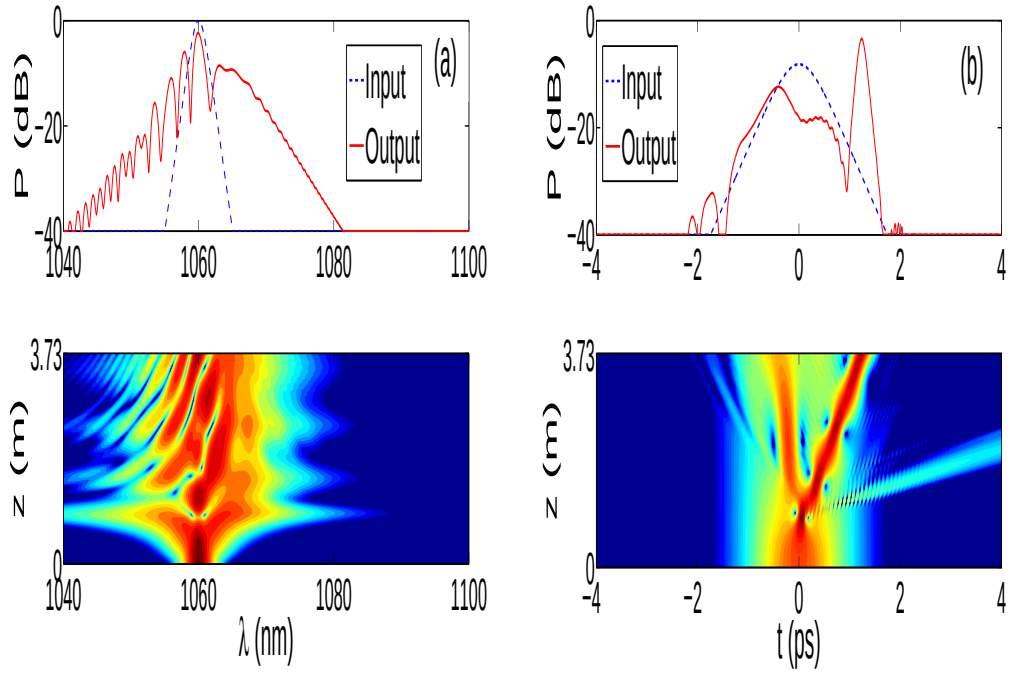

Figure 3.3: Spectral (a) and temporal (b) evolution of a third-order soliton over one soliton period, with the inclusion of TOD.

fixed, it gets $N = 3$. Figure 3.2 presents the spectral and temporal evolution of a third order soliton over one soliton period. In contrast to the fundamental soliton, the soliton of order $N = 3$ experiences stages of compression and broadening of its spectral and temporal shape and, at the distance $z_{sol} = 3.73$ m, it recovers its initial shape.

3.1.2 Third-order dispersion

The inclusion of third-order dispersion (TOD) in the propagation of soliton pulses in optical fibers is taken into account through the addition of the TOD term into equation (3.5), that is:

$$\frac{\partial A}{\partial z} + \frac{i}{2}\beta_2 \frac{\partial^2 A}{\partial t^2} - \frac{1}{6}\beta_3 \frac{\partial^3 A}{\partial t^3} = i(\gamma_a + \gamma_s) \mid A \mid^2 A. \tag{3.9}$$

Figure 3.3 shows the spectral (a) and temporal (b) evolution of a higher-order soliton of $N = 3$ as it propagates in a HC-PBGF over one soliton period. TOD is included in the propagation by using $\beta_3 = 2.6678$ ps^3/km. As we can see, the main effect of TOD on the evolution of the higher-order soliton is the interruption of its periodic behavior. At certain distance, the soliton breaks into sub-pulses. Such a break is known as soliton fission; and it can be seen in the temporal evolution shown in Figure 3.3(b), wherein we clearly note two pulses. In addition, from Figure 3.3a, the spectral evolution of the pulse shows an oscillatory behavior in the region of lower wavelength as long as it propagates along the fiber.

3.1.3 Intrapulse stimulated Raman scattering

The periodic nature of higher-order solitons is also disturbed when their propagation is subjected to the influence of the intrapulse stimulated Raman scattering (ISRS). Its inclusion into the NLSE is given by the integral terms in the equation:

$$\begin{aligned} \frac{\partial A}{\partial z} + \frac{i}{2}\beta_2 \frac{\partial^2 A}{\partial t^2} &= i\gamma_a(1 - f_a) \mid A \mid^2 A + i\gamma_s(1 - f_s) \mid A \mid^2 A \\ +i\gamma_a f_a A \int_{-\infty}^{+\infty} dt' R_a(t') \mid A(t - t', z) \mid^2 &+i\gamma_s f_s A \int_{-\infty}^{+\infty} dt' R_s(t') \mid A(t - t', z) \mid^2, \end{aligned} \tag{3.10}$$

The ISRS effects are included by the coefficients: for the silica: $\tau_1^s = 12.2$ fs, $\tau_2^s = 32$ fs and $f_s = 0.18$; and for the air: $\tau_1^a = 62$ fs, $\tau_2^a = 77$ fs and $f_a = 0.5$. Figure 3.4 presents the spectral (a) and temporal (b) evolution of a soliton under the influence of the ISRS. From 3.4(a), firstly we can see that, at certain distance, the ISRS induces the soliton fission, and secondly the continuous redshift of the

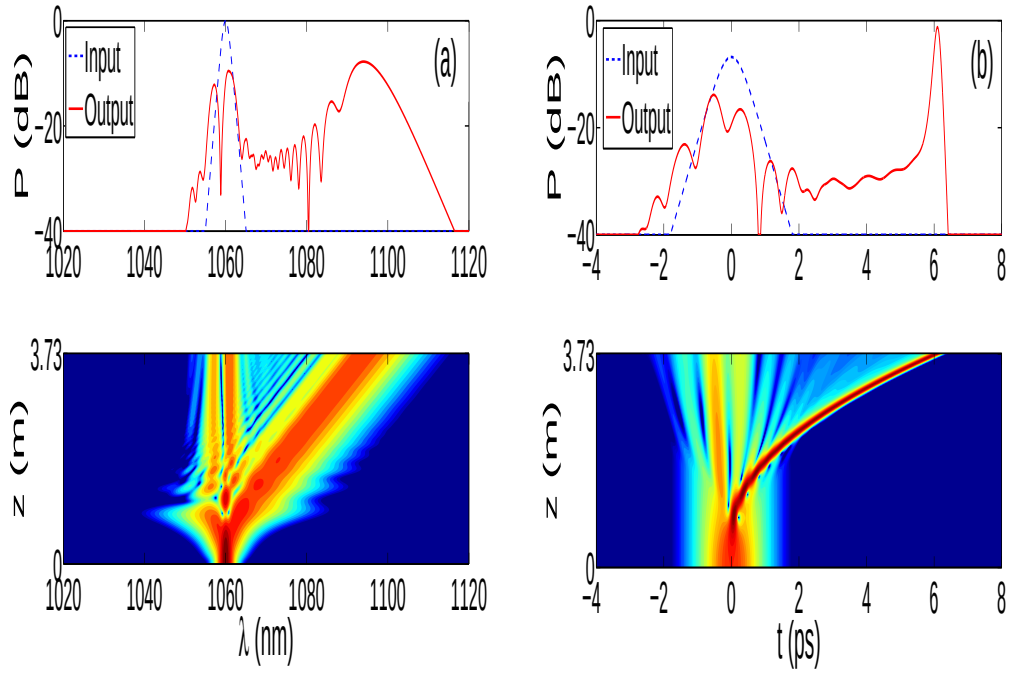

Figure 3.4: Spectral evolution (a) and temporal evolution (b) of a third-order soliton over one soliton period, with the inclusion of ISRS.

fissioned fundamental soliton. Such a redshift is a characteristic effect of ISRS and is called soliton self-frequency shift. Its physical origin comes from the delay nature of the Raman response. It also can be seen that the input soliton is broken into its three soliton components.

3.1.4 TOD and ISRS

In order to model accurately the evolution of a soliton, it is necessary to include both the higher-order dispersion and the ISRS effects since, in the femtosecond regime, these are the main effects that cause soliton fission. Figure 3.5 presents the evolution of a higher-order soliton of $N = 3$ using Equation 3.1 with k=3. Once again the

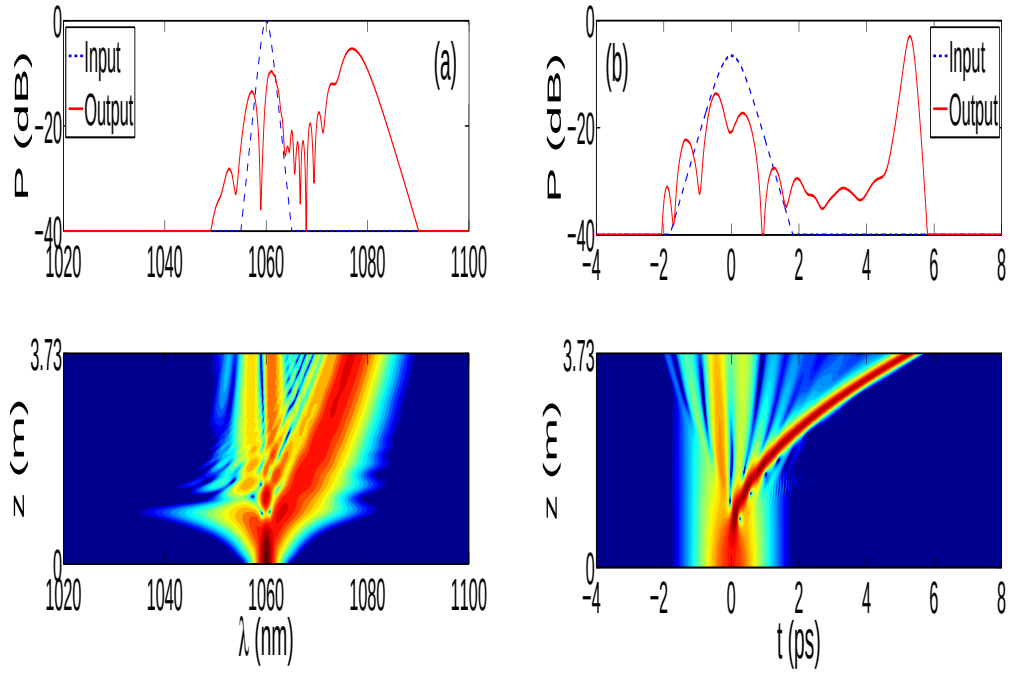

Figure 3.5: Spectral evolution (a) and temporal evolution (b) of a third-order soliton over one soliton period, with the inclusion of TOD and ISRS.

third-order soliton is fissioned into its three components and the fundamental soliton is redshifted. The effect of the TOD is such that it slows down the soliton redshift as we can see from the Figure 3.5(a).

3.2 Applications

We can make use of the dynamics of higher-order solitons in fiber optics either to compress or to shift in frequency an input pulse with the advantage that the fiber itself works either as a compressor and as a frequency shifting device, respectively.

In the case of pulse compression, as it was mentioned above, the higher-order

soliton undergoes periodic evolution patterns in which the soliton pulse experiences an initial narrowing phase. Thus we can choose the appropriate lenght of the fiber in order to achieve a compressed pulse with a particular or optimal compression factor, which is related to the peak power of the initial pulse. The fiber compressor device thus made is called soliton-effect compressor.

Let's now define the useful physical parameters that characterize a pulse compressor device. Firstly the pulse compression is quantified by the compression factor that is defined by [69]:

$$F_C = \frac{t_{FWHM}}{t_{comp}}, \tag{3.11}$$

where t_{FWHM} and t_{comp} are the full-width at half maximum (FWHM) of the input and output compressed pulses, respectively. Secondly the optimum lenght corresponds to the location at which the central spike reachs its minimum temporal value. The following empirical relation for the optimum length is used [74]:

$$z_{opt} = \frac{\pi}{2}\left[\frac{0.32}{N} + \frac{1.1}{N^2}\right] L_D, \tag{3.12}$$

where L_D is the dispersion length [71]. This previous expression has been proved extensively in standard optical fibers for values for the soliton order, N, up to 50 and, recently, in hollow-core fibers with good aproximation to the experimental values [75].

During the propagation of higher-order solitons along the fiber, some of the energy of the initial soliton pulse is distributed on the base of the pulse forming a broad pedestal in the output compressed pulse. Hence, for technological applications, not only pulses with higher compression factors are desirable but also pulses with a pedestal containing a minimum of energy. For such a reason, it is important

to introduce a parameter which gives information about the quality of the compressed pulse. The quality factor, Q_C, accomplishes such a task and is defined as the fraction of energy that is contained in the output pulse with respect to that of the input pulse, that is

$$Q_c = 1 - \frac{E_{\text{pedestal}}}{100}, \tag{3.13}$$

where E_{pedestal} is the pedestal energy that gives the percentage of the total input energy that is contained in the pedestal of the output (either compressed or shifted) pulse. It is defined as [76]:

$$E_{\text{pedestal}} = \frac{\mid E_{\text{total}} - E_{\text{sech}} \mid}{E_{\text{total}}} \times 100, \tag{3.14}$$

where E_{total} is the total energy contained in the output pulse and E_{sech} is the energy of a hyperbolic-secant pulse having the same peak power and FWHM as the output pulse.

The second application that makes use of the dynamics of higher-order solitons in fiber optics is related to the self-frequency shift of the pulse that is induced by the ISRS. Such a frequency shift depends on mainly two parameters: the soliton order of the input pulse and the non linear parameter of the optical fiber. In this work, the quantification of the SSFS is done by obtaining the final increment, Δ_λ, of the central wavelength with respect to that of the initial pulse.

4 Results

In chapter 2, the qualitative behavior that the spatial parameters of a HC-PBGF experience due to the increase or decrease of its cross section size was analyzed. Furthermore, in chapter 3, it was seen that higher-order solitons show stages of compression and broadening of its spectral and temporal shape as they propagate along the fiber,and, at the distance called soliton period, it recovers its initial shape. In the presence of perturbation, the periodic behavior of the higher-order solitons is interrupted, provoking soliton fission and then soliton self-frequency shift (SSFS).

Now, in this chapter, these phenomena, soliton pulse compression (SPC) and SSFS, are investigated under the influence of variations of the characteristics of the fiber and the input soliton pulse, focusing in the quality of the output pulses. It is worth to mention that SPC and SSFS are non linear phenomena that can take place in HC-PBGFs and that are in continuous investigation in order to find new light sources with specific characteristics. In particular, this chapter presents results obtained for both non linear phenomena in a proposed seven-cell HC-PBGF by solving the generalized non linear Schrödinger equation.

Thus two numerical studies are presented: the first one presents a numerical investigation on SPC and the impact of the variation in the cross section size of the fiber. And the second one performs a numerical investigation of low-order soliton

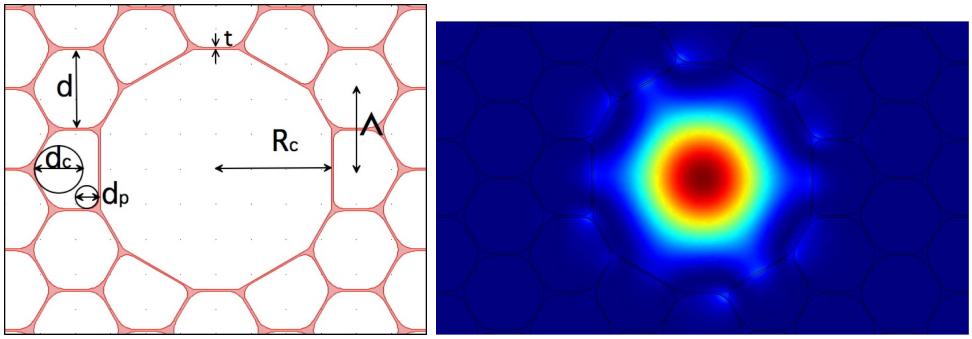

Figure 4.1: Cross section and fundamental air-guided mode of the modeled HC-PBGF. The colored (white) areas indicate silica (air) regions.

evolution in order to analyze the pulse quality in soliton pulse compression and SSFS in three fiber structures with different cross section sizes.

4.1 Modeled HC-PBGF

The modeled HC-PBGF structure consists of a triangular lattice of rounded hexagonal holes and an air core formed by seven-missing hexagonal unit cells as it is shown in Figure 4.1. The fiber transmission behavior is ruled by its geometry parameters, such as the hole diameter, d, the pitch, Λ, the diameter of curvature at the corners, d_c, the circle diameter, d_p, the silica ring thickness, t, and the core size, R_c. The core design of the fiber has a direct impact on the modal properties of the fiber. In this way, the rounded hexagonal holes in the structure of the fiber were chosen mainly for two important reasons: firstly, they increase the width of the transmission band of HC-PBGFs [68], and, secondly, their shape is typically that founded in commercial fibers.

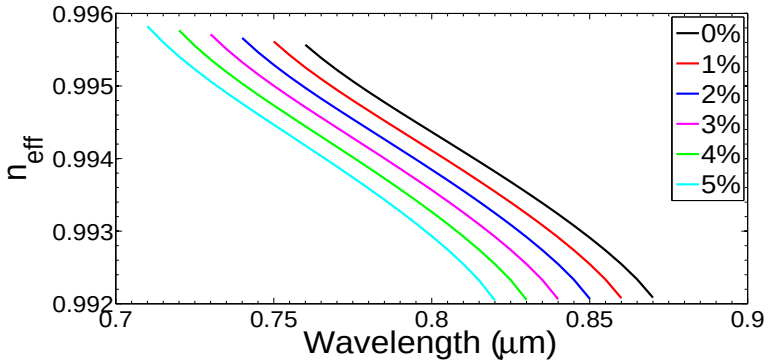

Figure 4.2: Effective index as a function of the wavelength from 0 to 5% of tapering factor for the studied structure.

4.2 Soliton pulse compression

In this section a numerical study of soliton pulse compression in a seven-cell HC-PBGF (shown in Figure 4.1) is presented. The enhancement of both the compression factor and the pulse shape quality of 360 nJ femtosecond pulses at the wavelength of 800 nm by tuning the cross section size of the fiber is investigated. Let's consider a hyperbolic secant input pulse in the form

$$A(0,t) = \sqrt{P_0}\,\mathrm{sech}\,(t/t_0), \tag{4.1}$$

with characteristics values of $\mathrm{P_0} = 3.6 \times 10^5\,\mathrm{W}$ and $t_0 = 500\,\mathrm{fs}$ for the peak power and the half width of the input pulse, respectively.

4.2.1 Influence of tuning the HC-PBGF

Let's study the effects of tuning the cross section size of the fiber on dispersion and non linear parameters, which are key features to take into consideration because they determine both the quality and the compression factor of the pulse. Firstly,

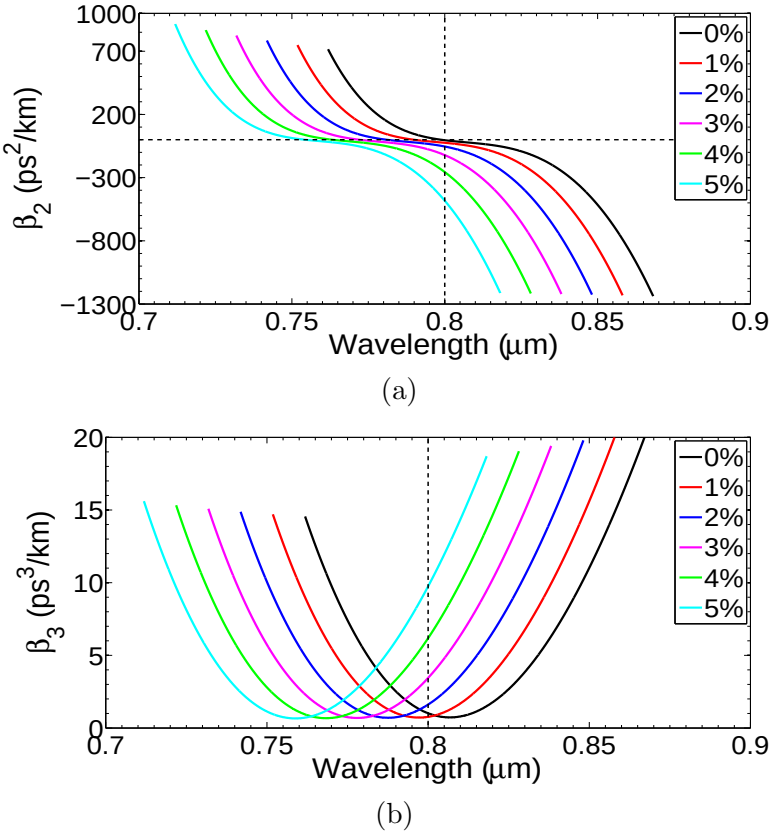

Figure 4.3: Second- (a) and third-order (b) dispersion parameters as a function of wavelength at different tapering factors.

both the working wavelength at 800 nm and the initial cross section of the fiber are defined. The main geometric parameters of the original structure were: $d = 1.92\mu$m, $\Lambda = 1.97\mu$m, $d_p = 0.51\mu$m, $d_c = 1.03\mu$m and $R_c = 2.82\mu$m. Let's tune (vary) the cross section size of the fiber and obtain the behavior of the dispersion and non linear parameter. This tuning is quantified by the tapering factor, which is defined as the percentage of reduction of the cross section size of the fiber with respect to its original value.

From Figure 4.2, it can be seen that the HC-PBGF without tapering presents

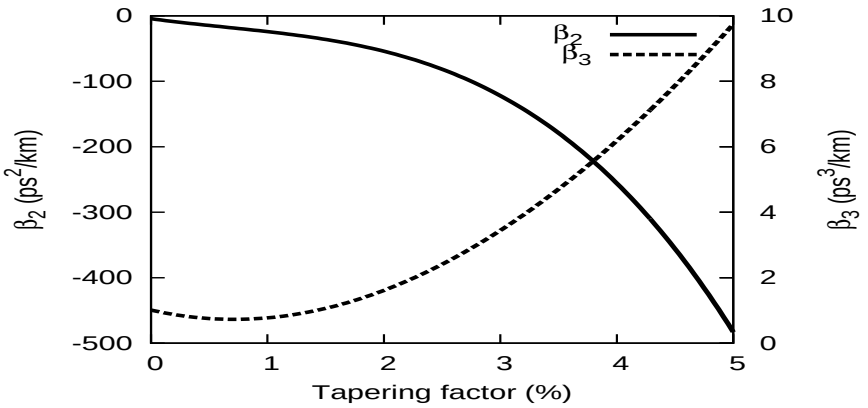

Figure 4.4: Second- and third-order dispersion parameters as a function of tapering factor at 800 nm.

fundamental air-guided modes from 760 nm to 870 nm, which represents a transmission bandwidth of 110 nm. As long as the tapering factor gets increased, the allowed modes shift to lower wavelengths. For a tapering factor of 5% the transmission bandwidth goes from 710 to 820 nm.

The second- (a) and third-order (b) dispersion parameter as a function of wavelength at different tapering factors are depicted in Figure 4.3. For all the studied structures, the second-order dispersion parameter presents an anomalous behavior in most wavelengths within the transmission bandwidth. In particular, for the wavelength of interest in this work, 800 nm, it can be observed that as the tapering factor increases, the second-order dispersion takes more negative values and the upper limit of the transmission bandwidth, of the air-guided mode, approaches to such wavelength (see Figure 4.3a). Meanwhile, the third order dispersion parameter is shown in Figure 4.3b. The first feature that it can be pointed out is that β_3 is positive for all the wavelength range. Furthermore, as the tapering factor increases, β_3 also increases, at the wavelength of 800 nm.

The dispersion parameters as a function of tapering factor are shown in Figure

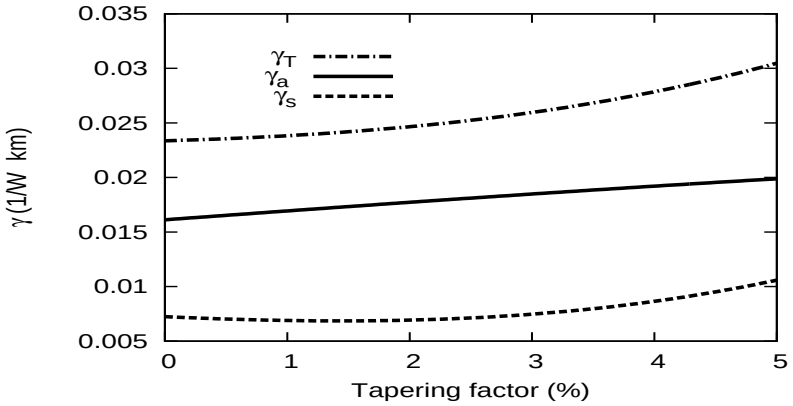

Figure 4.5: Contribution to the total non linear parameter from the silica and from the air as a function of tapering factor.

4.4, at a wavelength of 800 nm. It can be observed, from Figure 4.4, that the second-order dispersion $\beta_2 = -4$ ps^2/km for the untapered HC-PBGF, decreases with negative values as the tapering factor increases. For tapering factors $\geq 2\%$, β_2 takes values away from zero and decreases quickly. For example: $\beta_2 = -53$ ps^2/km when the tapering factor is 2% and decreases until $\beta_2 = -483$ ps^2/km for a tapering factor of 5%. On the other hand, the TOD parameter, β_3, becomes a monotonically increasing function for percentages of the tapering factor greater than one. A positive and large value of TOD has a deleterious effect on pulse compression which, in turn, make the quality of the pulse get reduced. So it is necessary to monitor their behavior as a function of the tuning of the cross section size of the fiber. This can be done through the relative dispersion slope, RDS, that is defined as the ratio between the third-order dispersion parameter and the absolute value of the second-order dispersion parameter, and is shown in Figure 4.6. The behavior of RDS can be divided in two regions: for tapering factor dimensions lower and greater than 1 %. In the former region, the RDS decreases quickly from values of 100 fs to values around 30 fs; meanwhile, in the latter region, it keeps close to values around 25 fs.

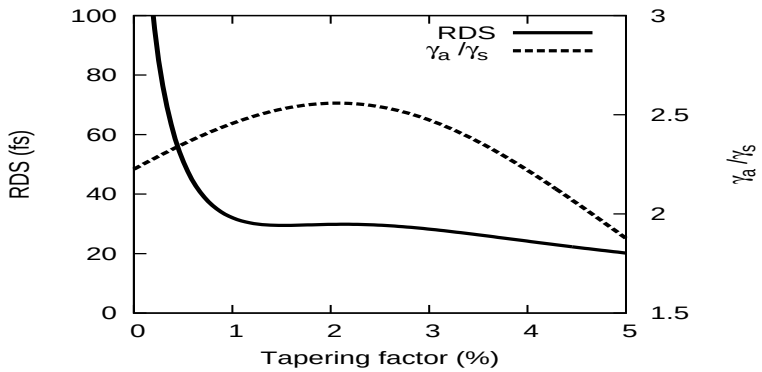

Figure 4.6: Relative dispersion slope, RDS, and ratio between the non linear parameters of air (γ_a) and silica (γ_s) as a function of the tapering factor.

We can see from Figure 4.5 the silica and air contributions to the non linear parameter as well as the total non linear parameter as a function of the tapering factor. The main contribution to the total non linear parameter comes from the air regions. The total non linear parameter, γ_T, shows an increasing behavior, with values around 0.025 1/(W km), as the tapering factor increases. Figure 4.6 also shows the ratio of γ_a/γ_s. It presents an increasing behavior for tapering factors lower than 2%, whereas it decreases for larger values. However, in almost all the tapering factor range shown in the figure, their values remain in the range between 2 and 2.5, which means that the contribution of air to the non linear parameter is approximately twice the value of that corresponding to the contribution of silica.

4.2.2 Pulse shape quality

In order to improve the pulse shape quality, let's chose tapering factors larger than 2 % since according to Figure 4.6, in this range, the RDS reaches smaller values. Results are only presented for tapering factors less than 5%; for higher values, there is no fundamental guided mode at 800 nm because the transmission band of the corresponding HC-PBG fiber structure shifts towards lower wavelengths due to the

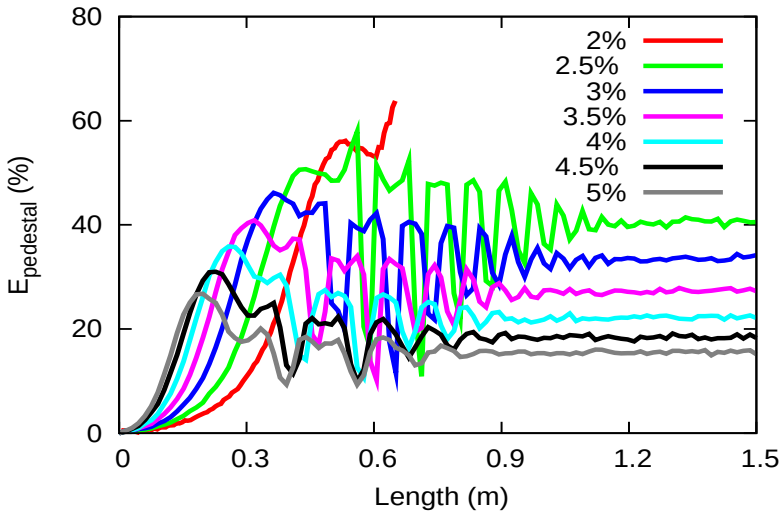

Figure 4.7: Pedestal energy of the pulse as it propagates along the fiber as a function of propagation length and for different tapering factors.

tuning of the cross section size of the fiber [77]. As it is shown next, greater values of RDS result in a poor pulse shape quality. This can be observed in Figure 4.7, wherein it is shown the way in which a light pulse develops a pedestal energy as it propagates along the fiber for different tapering factors. For a given tapering factor, the pedestal energy monotonically increases, reaching its maximum value at a particular distance, from which it gets decreased and starts showing an oscillatory behavior. At a particular length, the pedestal energy keeps having almost unchanged values, indicating the formation of the fundamental soliton, which is fissioned from the induced higher-order soliton. On the other hand, we can also observe from Figure 4.7 that the maximum of the pedestal energy increases as the tapering factor decreases. The lower value of the maximum of the pedestal energy, which is around 25%, is found for a tapering factor of 5% and for a length of around 0.2 m. It is also important to underline, for instance, that for a tapering factor of 2%, which have a value of RDS at around 30 fs, the pedestal energy reaches significant values that are

a detriment to the pulse shape quality.

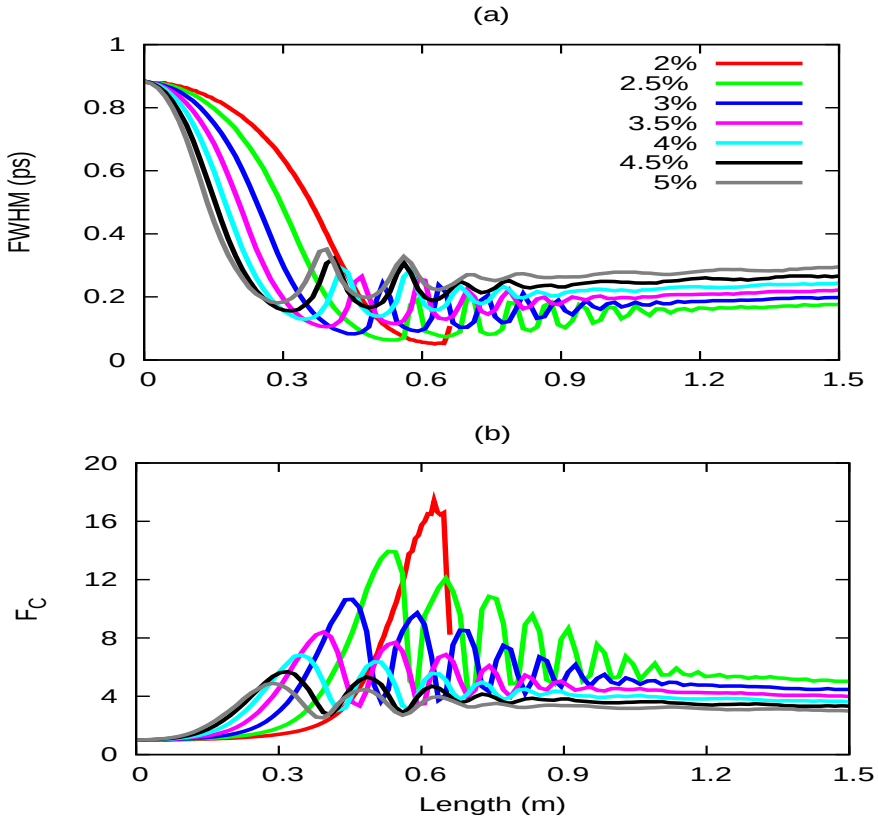

Figure 4.8: Full width at half maximum (a), FWHM, and compression factor (b) as a function of the propagation length of a pulse and for different tapering factors.

Figure 4.8(a) shows the FWHM of pulses as a function of the propagation distance and for different tapering factors. We can observe that, for a given tapering factor, the pulse experiences a first stage of compression in which the FWHM of the pulse reaches their minimum temporal value at a particular propagation length. At a second stage, the FWHM of the pulse shows and oscillatory behavior and finally, it gets an almost constant value, indicating the formation of red shifted solitons. Such solitons are fundamental solitons that arise as a consequence of the soliton

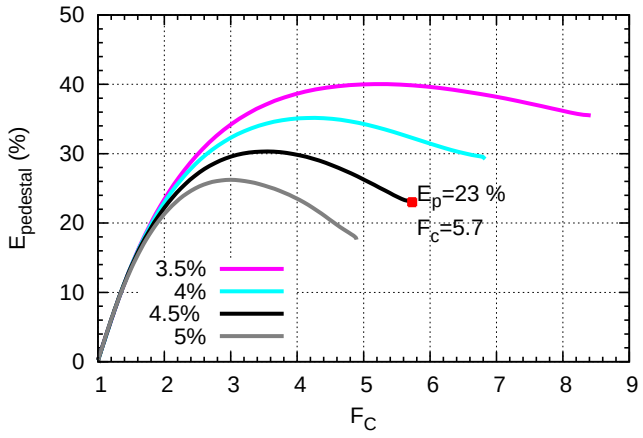

Figure 4.9: Pedestal energy as a function of compression factor for the HC-PBGFs with better pulse shape quality

fission. Besides, it can also be seen from Figure 4.8(a) that the minimum temporal width is reached at shorter distances as the tapering factor increases (or RDS decreases). In Figure 4.8(b), it can be seen the compression factor as a function of the propagation distance and for different tapering factors. For a given tapering factor the compression factor behavior is such that it increases with propagation distance until it reaches its maximum value. On the other hand, the maximum of each compression factor curve decreases as the tapering factor increases and it is found at shorter propagation lengths. This behavior is explained as follows: the temporal width of the soliton is proportional to β_2; thus the more negative the β_2 value is, the greater the temporal width is. This statement is reflected on the behavior of the lower value of the minimum of the FWHM of the curves of Figure 4.8. It is gotten for a tapering factor of 5% and at shorter propagation distance. At such tapering factor, the second-order dispersion has the greatest value. Hence, the compression factor must get its maximum more decreased for a tapering factor of 5% and be found at a shorter propagation length.

In order to evaluate the best option of optical fiber for pulse compression, it is necessary to take into account both features, the compression factor and the pedestal energy of a propagating pulse. Hence, it is desirable to have a pulse that have the greater compression factor and, simultaneously, the lower pedestal energy in order to have a better pulse shape quality. From Figure 4.8(b), on the one hand, it can be observed that higher pulse compression factors arise for fibers with the lower tuning factors. On the other hand, from Figure 4.7, we can see that the pulse develops a pedestal energy during its propagation along the fiber. The pedestal energy can reach values greater than 40%. In such a case, the quality of the pulse shape is seriously compromised. It can also be observed from Figure 4.7 that the compressed pulse develops the lower pedestal energy ($< 40\%$) when it propagates in HC-PBGFs with tuning factors of 3.5, 4, 4.5 and 5%. Figure 4.9 shows the behavior of the pedestal energy as a function of the compression factor for these tuning factors. When the pedestal energy reaches a value of 20%, the compression factor is around 1.8 for all fibers. For compression factors above 1.8, the pedestal energy increases as the tapering factor decreases. We consider that a good choice of fiber structure for pulse compression can be that wherein a pulse propagates and develops pedestal energies with values $\leq 30\%$. With such standard of quality, the HC-PBGFs with tapering factors of 3.5% and 4% are discarded due to their high pedestal energy values, 30-40%, although their compression factors reach values greater than 6. Thus, the better choices for pulse compression are those fibers with tuning factors of 4.5% and 5%, which promote output compressed pulses with compression factors and pedestal energies of $F_c = 5.7$ and $E_p = 23\%$, $F_c = 4.9$ and $E_p = 18\%$, respectively. However, the best choice is that fiber structure characterized by a tapering factor of 4.5%, as it is shown in Figure 4.9, since in that structure the pulse has the greatest pulse shape quality (or lower pedestal energy) along with the highest compression factor. In Figure 4.10, the optimum output compressed pulses are depicted for HC-

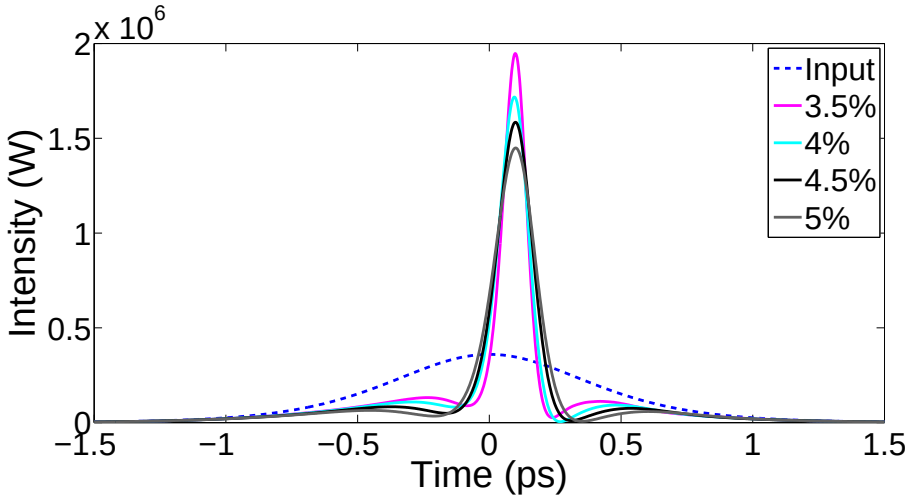

Figure 4.10: Temporal pulse shape of the optimum output compressed pulses for HC-PBGFS with tapering factors from 3.5 to 5%.

PBGFs with tapering factors from 3.5 to 5%. It can be seen that the energy of the output compressed pulses is mainly distributed in its center; the pedestal energy, in contrast, is distrubuted in the edges. It can also be observed that, as the tapering factor increases, both the compression factor and the pedestal energy also increase, as it was previously described.

Figure 4.11 shows both the temporal and the spectral shape of the input and optimum compressed pulses. The corresponding compression factor has the value of 5.7 and it has a pedestal energy value of $E_{pedestal} = 23\%$, as it is shown in Figure 4.9. Such a compression factor is reached only after the pulse has been propagated through a distance of 31 cm (see Figure 4.8(b)). The above compression factor result is worthy of note: if we compare it with respective values found in previous works, then it can be seen that, although higher compression factors are achieved, they are obtained at several meters of propagation of the pulse along the HC-PBGF.

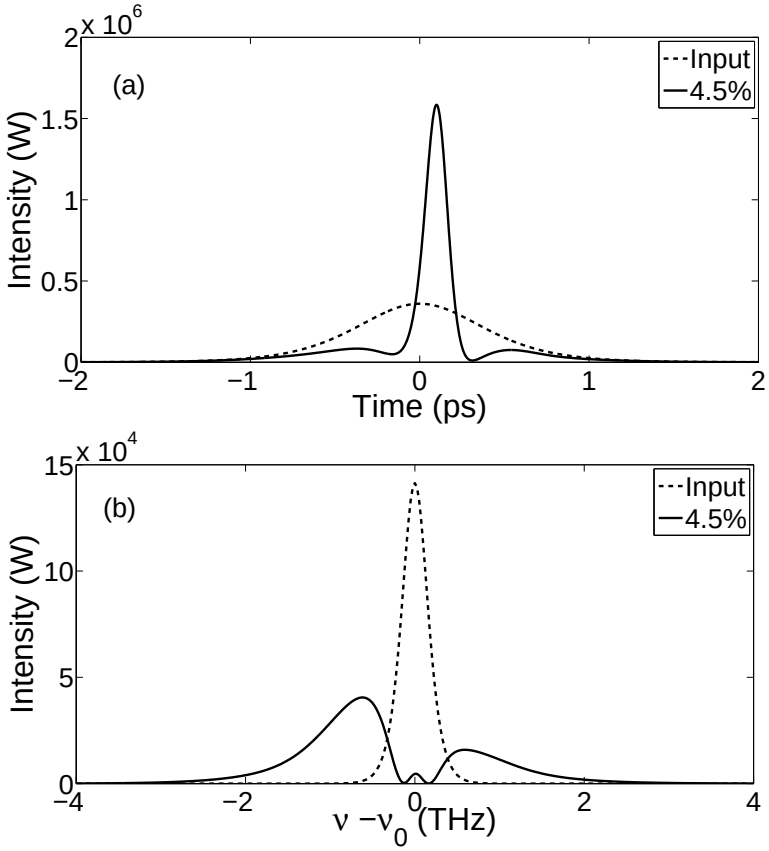

Figure 4.11: Temporal pulse shape (a) and frequency spectrum (b) of the optimum compressed pulse for a HC-PBGF with tapering factor of 4.5%.

4.2.3 Conclusions

We have studied numerically the influence of tuning the cross section size of a seven-cell hollow-core photonic bandgap fiber on both the pulse shape quality and the compression factor for unchirped pulses of 500 fs (or 881.5 fs of FWHM). It was found that a tuning of the cross section size of the fiber with a tapering factor of 4.5% improves both features. Our numerical results indicate a maximum compressed pulse with a compression factor of 5.7 with a temporal FWHM of 153.8 fs. The pulse reaches a peak power of 1.5851 MW with 77% of pulse shape quality. The length of

the fiber at which the compressed pulse is reached is of 31 cm. To my knowledge, higher compression factors have only been obtained by using several meters of HC-PBGFs. Here, the present results show that, with an appropriate tuning of the cross section size of HC-PBGF, pulse compression can be improved significantly.

4.3 Soliton self-frequency shift

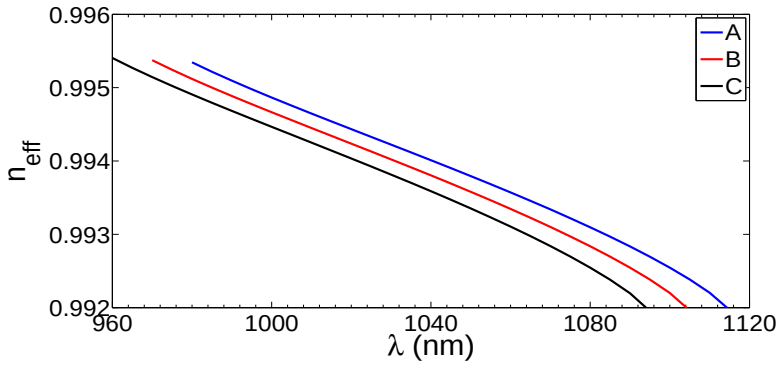

Figure 4.12: Effective index as a function of wavelength for the A, B and C structures.

In this section a numerical investigation of low-order soliton evolution in the proposed seven-cell HC-PBGF shown in Figure 4.1 is reported. In the numerical simulation, the pulse quality evolution in soliton pulse compression and soliton self-frequency shift is investigated in three fiber structures with different cross section sizes. In the simulation, unchirped soliton pulses, of 400 fs, at the wavelength of 1060 nm are considered. In the analysis, let's consider a hyperbolic secant input pulses in the form of equation (4.1) where the peak power takes values in such a way that the corresponding input soliton orders are $N = 1.5, 2, 2.5, 3$ and $t_0 = 400\,\text{fs}$ is the input-pulse width.

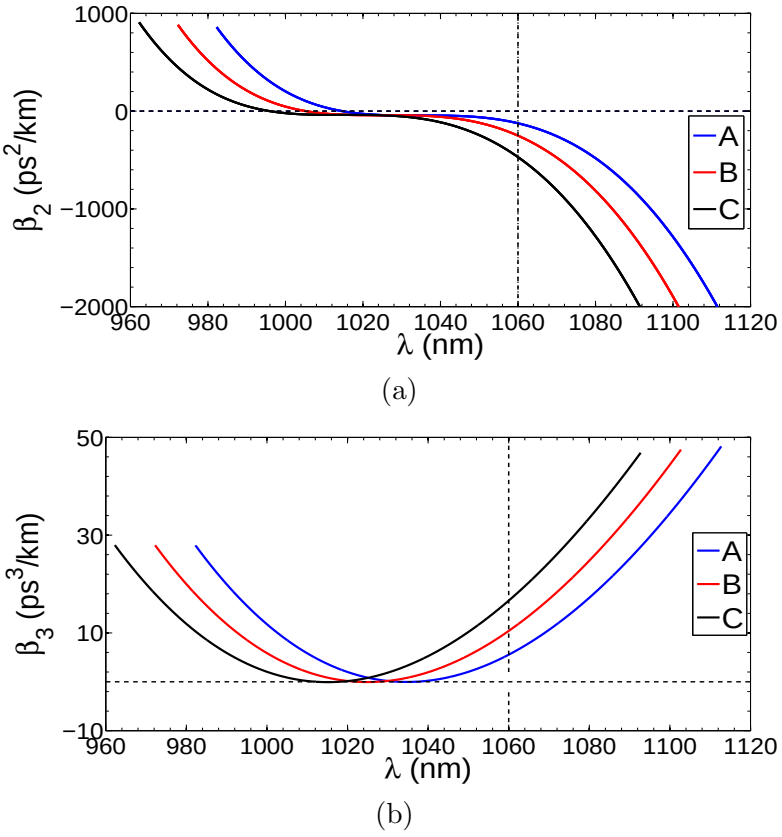

Figure 4.13: Second- (a) and third-order (b) dispersion parameters as a function of wavelength for the A, B and C structures.

Three HC-PBGF structures, namely A, B and C, are studied. The A fiber structure has the following main initial parameters: $d = 2.46$ μm, $\Lambda = 2.53$ μm, $d_p = 0.66$ μm, $d_c = 1.32$ μm and $R_c = 3.61$ μm. Meanwhile, the cross section size of the B and C fiber structures have been reduced to 1 and 2 %, respectively, with respect to that of the A structure. In other words, we consider that the fiber preserves its original form and geometry and only experiences an uniform decrease of its transversal dimensions.

Effective index as a function of wavelength for the three studied HC-PBGFs

are shown in Figure 4.12. For the A structure, fundamental guides modes are found within the wavelength range from 980 nm to 1112 nm; meanwhile, for the B structure they are found from 970 nm to 1104; and for the C structure, the fundamental guided modes are found from 960 nm to 1094 nm.

Second- and third-order dispersion parameters as a function of wavelength for the studied structures are depicted in Figure 4.13. The transmission bandwidth is $\approx$ 130 nm. Most of the allowed wavelengths are in the anomalous region. The zero-dispersion wavelengths (ZDWs) for the studied HC-PBGFs are located at 1015, 1005 and 995 nm, respectively. In addition, the second-order dispersion parameter values, for the A, B, and C fiber structures, at $\lambda_0 = 1060$ nm, are the following: -120, -245 and -457 ps^2/km, respectively. As expected, the effect of reducing the cross section size of the HC-PBGF is the shift of the ZDW to shorter wavelengths and, consequently, the second-order dispersion parameter, shown in Figure 4.13(a), takes more negative values. From Figure 4.13(b), it can be seen that β_3 presents the same qualitative behavior for the three structures. TOD curves shift to shorter wavelengths and the value of β_3 at 1060 nm gets increased as the cross section size of the fiber is reduced. Their corresponding β_3 values are the following: 5, 10 and 16 ps^3/km, respectively. The respective energy of input solitons with orders N =1.5, 2, 2.5 and 3 are: 125.5, 223.1, 348.6 and 501.98 nJ, for the A fiber structure; 240, 426, 666.51 and 960 nJ, for the B fiber structure; and .422, 0.751, 1.173 and 1.69 μJ for the C fiber structure, respectively.

We can see from Figure 4.14 the silica and air contributions to the total non linear parameter as a function of wavelength for the A HC-PBGF structure. Similar behavior of the non linear parameter for the B and C structures is observed. A reduction of the cross section size of the fiber of 1 and 2% induces an increment of the magnitude of γ_T, at the wavelength of 1060 nm, of 0.057 $\times 10^{-5}$ and 0.131

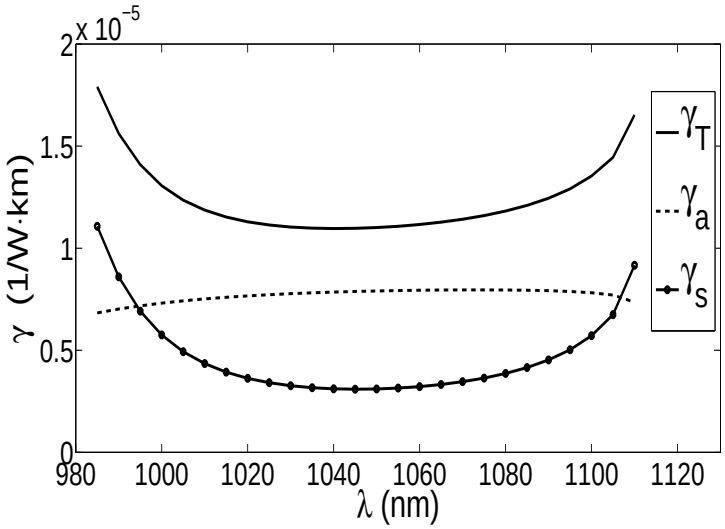

Figure 4.14: Non linear parameters contributions for the studied HC-PBGFs A structure as a function of wavelength. The total non linear parameter, γ_T, is given by the sum of the contributions of the silica, γ_s, and of the air, γ_a.

$\times 10^{-5}$ $1/(\mathrm{W}\cdot\mathrm{km})$, respectively. We observe that the main contribution to the non linear parameter comes from the air region. The principal feature of γ_T, seen in all corresponding curves, is the almost flat region that is present in the middle of the transmission bandwidth. In addition, there is an increase in both the low and the upper sides of the respective curves. Besides, γ_T takes higher values as the cross section size is reduced.

Figure 4.15 shows the relative dispersion slope for the three studied HC-PBGFs as a function of wavelength. It can be observed that the reduction of the cross section size of the HC-PBGF produces lower values for the RDS and a decrease of the wavelength range, within the anomalous region, wherein the input pulse can propagate. The latter can be understood recalling that the transmission window is shifted to shorter wavelengths due to the reduction of the cross section size of the HC-PBGF, as it can be seen from Figure 4.13. The transmission wavelength ranges

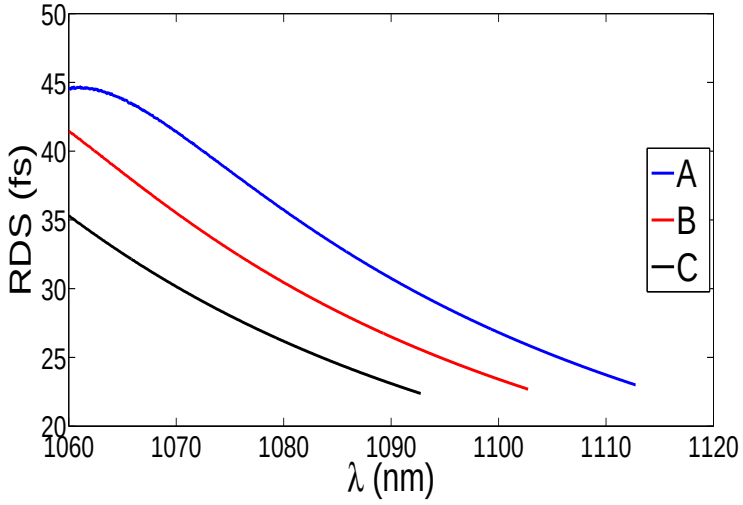

Figure 4.15: Relative dispersion slope, RDS, as a function of wavelength, for the three studied HC-PBGFs.

are ≈ 52, 42 and 32 nm for the A, B and C fiber structures, respectively.

Hence, a study of the evolution of a soliton pulse of order N, as it propagates along the HC-PBGF, is studied by taking into account the effects of second- and third-order dispersion, self-phase modulation and intra pulse Raman scattering. During the propagation, the pulse experiences an initial stage of compression (or a broadening of the spectrum) and, after some distance, it reaches maximum compression (or maximum bandwidth), which corresponds to the optimum length, z_{opt}, that indicates the onset of the soliton fission. The resultant sub-pulse undergoes stages of compression and broadening experiencing a continuous shift to longer wavelengths due to the Raman gain [78]. Then it follows the formation of a fundamental soliton which central wavelength keeps redshifting as it propagates along the fiber. This behavior can be seen, in detail, in Figure 4.16, which shows density plots for the temporal and spectral evolution of an input soliton pulse, of order $N = 2$, as it

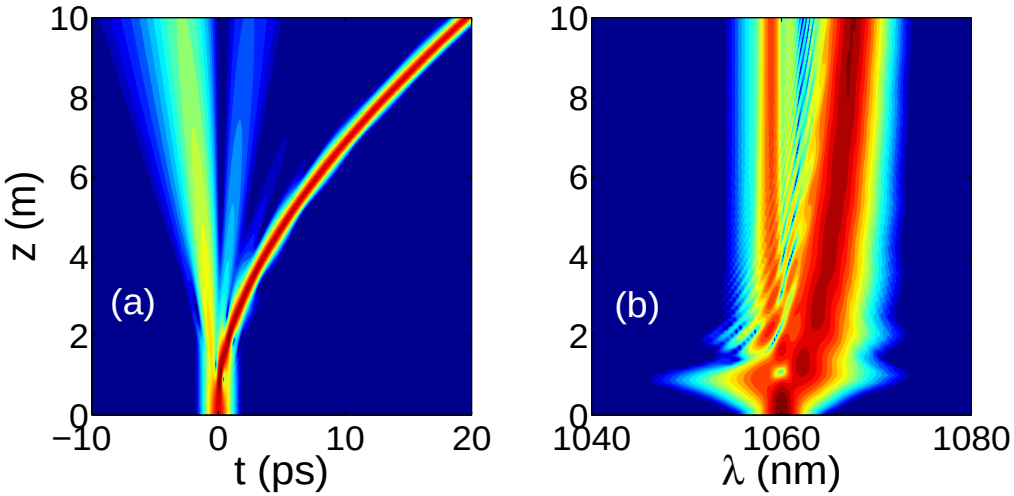

Figure 4.16: Density plots of the temporal (a) and spectral (b) evolution of an input soliton pulse of order $N = 2$, along a propagation length of ten meters, in a HC-PBGF.

propagates along ten meters of the A HC-PBGF. In the following, both the temporal and spectral evolution of a soliton pulse will be studied. Firstly, let's study the optimum compressed soliton pulse and, secondly, the maximum SSFS.

Figure 4.17 shows the compression factor experienced for the soliton pulse as it propagates through the different studied HC-PBGFs. The soliton pulse propagates and undergoes a first stage of compression in which it reaches a minimum temporal width at the optimum length, z_{opt} (see equation 3.12). Later, a second stage is observed, in which there is an oscillatory behavior of compression and broadening of the pulse width; and, finally, it follows a decreasing tendency indicating the formation of a fundamental soliton which is fissioned from the input pulse. We can also observe from Figure 4.17 that the maximum compression factor increases with a higher value of the soliton order.

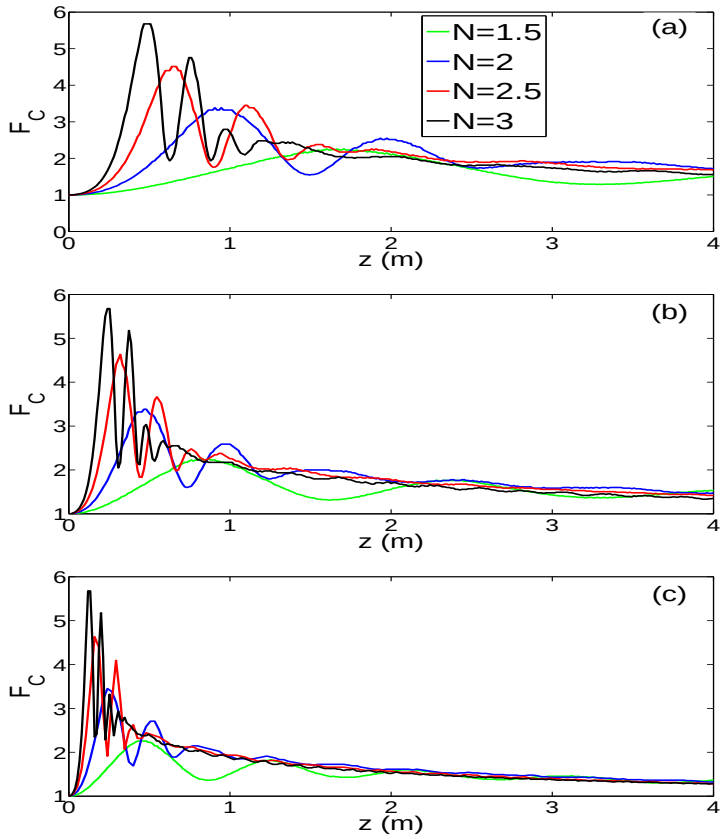

Figure 4.17: Compression factor as a function of the propagation length and of soliton number, N, for the studied HC-PBGFs: (a) A, (b) B, and (c) C .

Furthermore, it is worth to point out that the maximum values of the compression factor of the pulse in all three studied HC-PBGFs are approximately equal, but the propagation length at which those values are reached decreases as the soliton order increases, and the cross section size of the fiber is reduced (or for those structures with larger negative values of β_2).

Figure 4.18 shows the quality factors of the pulse as it propagates along the three HC-PBGFs. The behavior of the quality factor is such that it firstly decreases to a minimum value; then it experiences an oscillatory stage and, after certain distance,

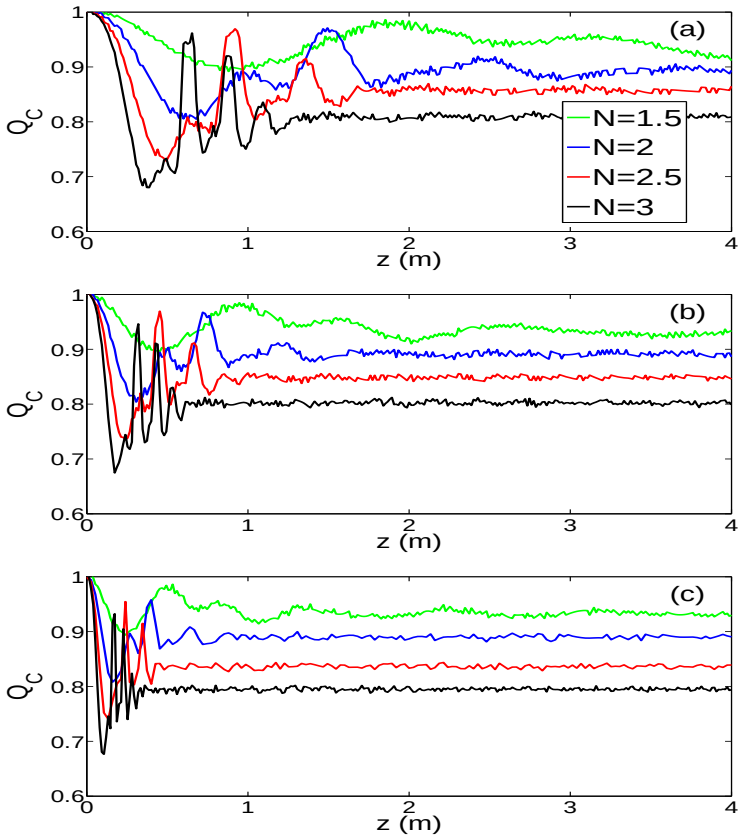

Figure 4.18: Pulse quality factor as a function of propagation length and of soliton number, N, for the studied HC-PBGFs: (a) A, (b) B, and (c) C .

it almost keeps a constant value. The first two stages correspond to the stages of compression and broadening of the initial pulse. Meanwhile, in the last stage, the formation of a fundamental soliton takes place. Another feature seen in Figure 4.18 is that higher-order input solitons results in, as an average, a general decrease of the quality factor, and a decrease of the distance at which the fundamental soliton is formed. For input solitons with orders of $N = 1.5, 2, 2.5$ and 3, the quality factors of the red shifted solitons is ≈ 0.94, 0.9, 0.85 and 0.8, respectively. Since, for higher-order input solitons, their quality factors are negatively affected, let's only present

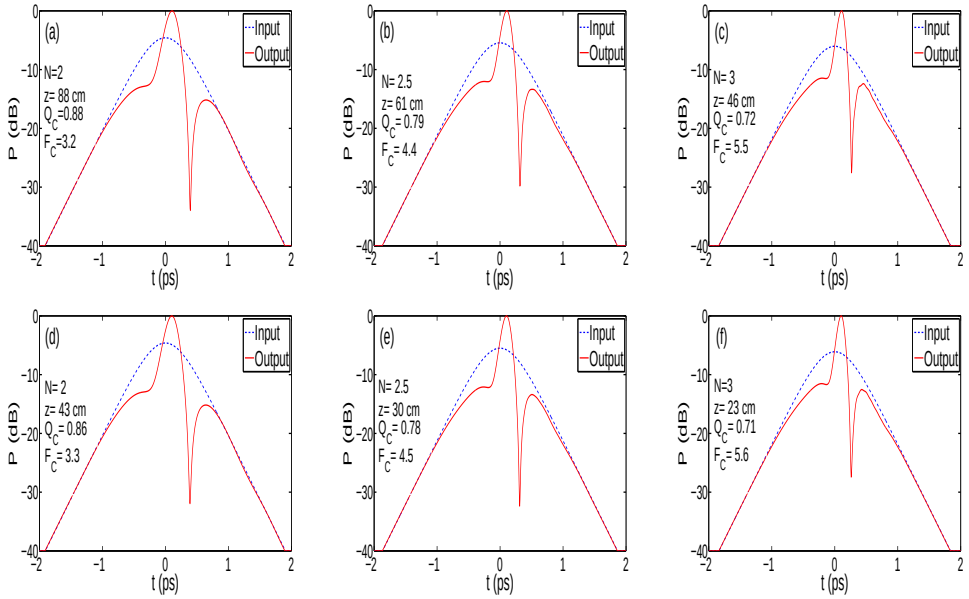

Figure 4.19: Output compressed pulses in the A (a)-(c) and B fiber (d)-(f) structures.

results for up to $N = 3$. It can be seen, from both Figure 4.18 and Figure 4.17, that in order to achieve higher compression factors, it is necessary to increase the value of the soliton order. However, by doing so, it results in a decrease of the quality of the compressed pulse.

This can be seen more clearly in Figure 4.19 where the optimum output compressed pulses are depicted for the A and B HC-PBGFs, for $N = 2, 2.5$ and 3. Considering an input pulse with a value of the soliton order of $N = 2$, the compression factor reaches a value of 3.2 with a pulse quality factor of 0.88 for the A fiber (see Figure 4.19(a-c)). Meanwhile, for an input soliton pulse of $N = 3$, it increases until 5.5; however, the pulse quality factor decreases to a value of 0.72. Similar behavior is observed for the compressed pulses for the B fiber structure (see Figure 4.19(d-f)).

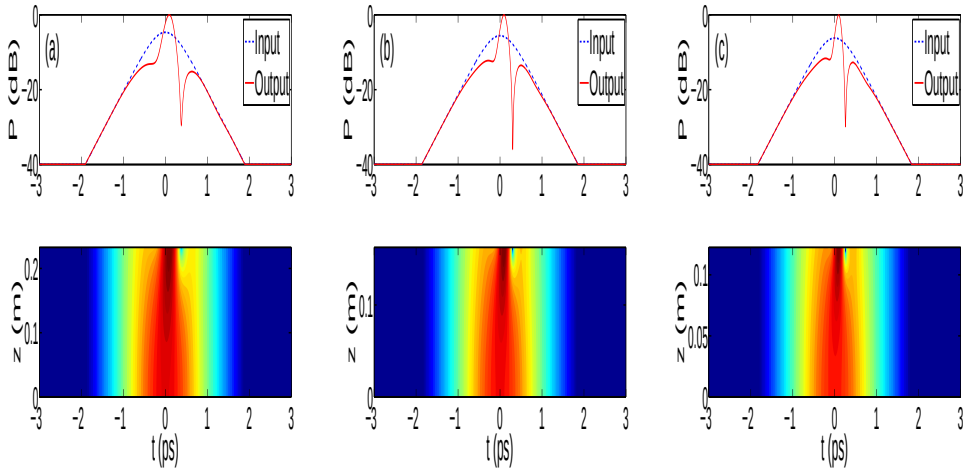

Figure 4.20: Upper panels: output compressed pulses as a function of soliton order: (a) $N = 2$, (b) $N = 2.5$ and (c) $N = 3$, for the C fiber structure. Lower panels: corresponding density plots of the temporal evolution of the soliton pulse.

The temporal evolution of the pulse as well as the output compressed pulse as a function of soliton order for the C structure is shown in Figure 4.20, for $N = 2, 2.5$ and 3. The propagation lengths at which the pulse reaches its maximum compression factor are: 23, 16 and 12 cm for soliton orders of 2, 2.5 and 3, respectively. And their quality (compression) factors are: $Q_C = 0.88$ ($F_C = 3.3$), $Q_C = 0.79$ ($F_C = 4.5$) and $Q_C = 0.73$ ($F_C = 5.6$), respectively. Table 4.1 summarizes the results obtained for the SPC in the three studied HC-PBGFs structures.

We can observe, in Figure 4.21, the spectra of the output-pulse power after 10 m of propagation length. If the input soliton number increases, the SSFS also does. For the A fiber structure, the soliton of order $N = 3$ reaches a central wavelength of $\lambda_0 = 1076.5$ nm. On the other hand, for the B fiber structure, the soliton of order $N = 3$ shows an improvement of the SSFS reaching a maximum central wavelength of $\lambda_0 = 1082.4$ nm.

Table 4.1: Output parameters of the optimum compressed pulse for the studied HC-PBGFs structures.

Structure	N	F_C	Q_C	z_{opt} (cm)
A	1.5	2.2	0.94	142
	2	3.2	0.88	88
	2.5	4.4	0.79	61
	3	5.5	0.72	46
B	1.5	2.1	0.93	71
	2	3.3	0.86	43
	2.5	4.5	0.78	30
	3	5.6	0.71	23
C	1.5	2.2	0.94	38
	2	3.3	0.88	23
	2.5	4.5	0.79	16
	3	5.6	0.73	12

In Figure 4.22, the spectra of the output-pulse density power for the C fiber structure can be seen. The soliton of order $N = 3$ reaches the largest SSFS after a propagation length of 6 m: $\lambda_0 = 1088.4$ nm. Such an improvement can be understood if we recall that the C structure presents higher values for its non linear parameter than those corresponding to the A and B fiber structures (see Figure 4.14). We can also see from Figure 4.22 that the higher value of the soliton order, the larger initial shift of the fundamental soliton is. After an initial stage of accelerated soliton redshift, it decelerates to a lower value. For example: for $N = 2$, after a propagation length of 5 m, the fundamental soliton redshifts 11.6 nm; meanwhile, in the following 5 m of propagation, it only redshifts 3.2 nm. It is worth to underline that, according to the results, if the soliton order is increased, the SSFS also does. Table 4.2 lists the output parameters of SSFS for input soliton pulses of order $N = 2, 2.5, 3$, respectively, for the three HC-PBGFs structures.

In summary, for soliton pulse compression, it has been observed that a reduction

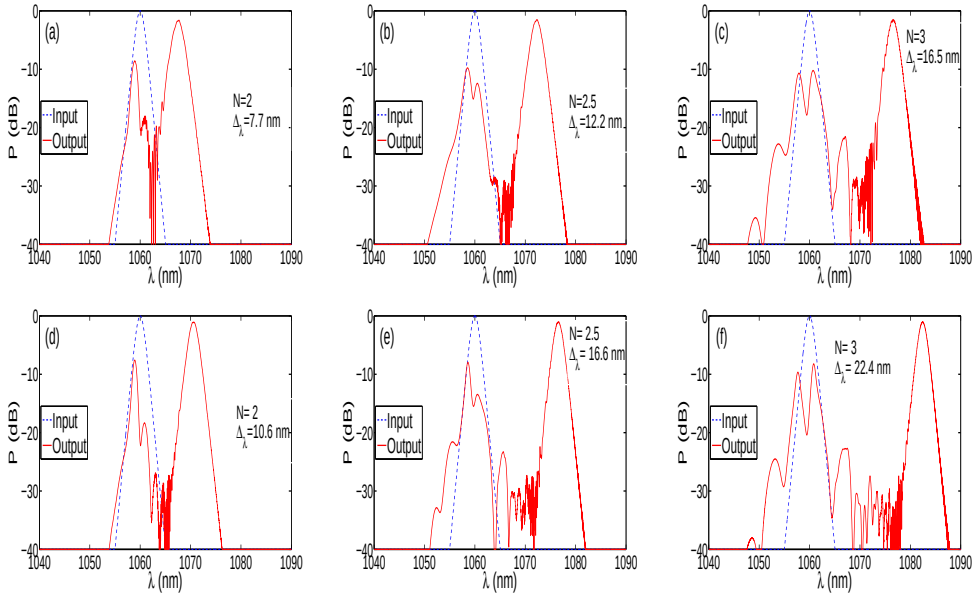

Figure 4.21: Spectra of the output-pulse power after 10 m of propagation in the A fiber structure (a)-(c) and B fiber structure (d)-(f). N is the soliton order and Δ_λ is the SSFS.

of the cross section size of the HC-PBGF results in that the second-order dispersion takes highly-anomalous values and, as a consequence, the optimum length for compression is reduced. The present results also show a well known behavior: the greater soliton order (higher power), the higher compression factor that is obtained. This has a cost in the compressed-pulse quality: high values of N results in a reduction in its quality. The impact of the non linear parameter on SSFS is clearly visible, since for the same order of soliton, the fiber structure wherein the SSFS is greater is that with the largest non linear parameter. On the other hand, it also seen that a larger SSFS is reached, at shorter propagation distance, when the order of the soliton takes greater values and the second-order dispersion is more highly anomalous. The input-soliton order influences on both the SSFS and the amount of energy that will be present in the output pulse, or energy conversion from the input

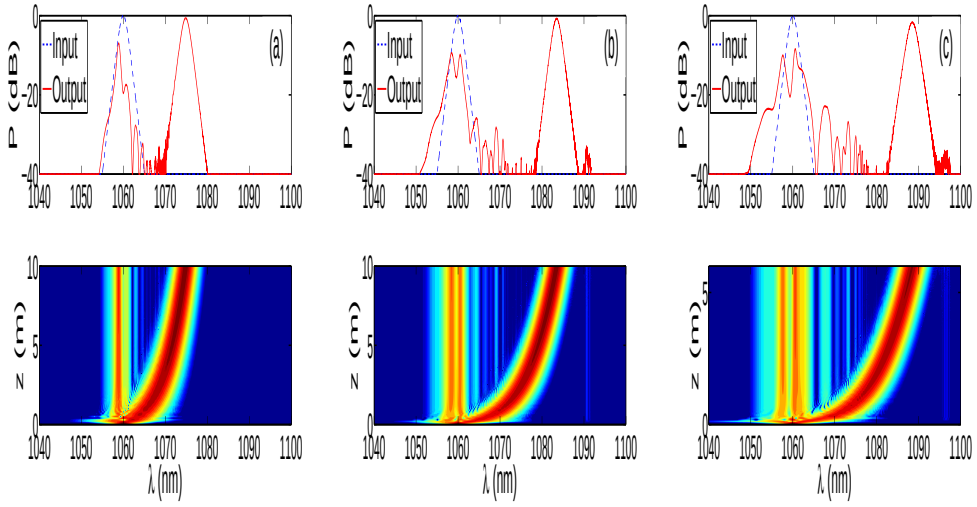

Figure 4.22: Spectra of the output-pulse power (upper panels) and density plots (lower panels) of the spectral evolution of input soliton pulses in the C fiber structure. The corresponding values of the soliton order and the propagation distance are the following: (a) $N = 2$, z=10 m; (b) $N = 2.5$, z=10 m; and (c) $N = 3$, z= 6 m.

to the output soliton pulse. It is important to note that a high value of the soliton order produces a reduction in the amount of energy contained in the shifted soliton pulse. However, the results show that for a value of $N = 3$, the output pulse will contain approximately 80% of the energy of the higher-order input soliton.

4.3.1 Conclusions

A numerical study of the low-order soliton evolution in a three hollow-core photonic bandgap fibers, which differ from each other in their cross section size, has been performed. Unchirped pulses of 400 fs of width and with central wavelength of $\lambda_0 = 1060$ nm were considered. The analysis was focused on the pulse quality evolution in SPC and SSFS. The results showed that the seven-cell HC-PBGFs, with a cross section size reduction of 2%, present larger anomalous values of the

Table 4.2: Output parameters of the soliton self-frequency shift for the studied HC-PBGFs structures, for $N = 2, 2.5$ and 3. The propagation length is $z = 10$ m except for the case wherein $N = 3$ for the C structure, which $z = 6$ m.

Structure	N	Δ_λ (nm)	Q_C
A	2	7.7	0.89
	2.5	12.2	0.86
	3	16.5	0.80
B	2	10.6	0.89
	2.5	16.6	0.85
	3	22.4	0.80
C	2	14.8	0.89
	2.5	23.4	0.85
	3	28.4	0.80

second-order dispersion and greater values of the non linear parameter. If an input soliton pulse with order of $N = 3$ (which corresponds to an energy of 1.69 μJ) propagates a distance of 12 cm, it gets compressed with a compression factor of 5.6 and quality factor of 0.73. Meanwhile, after the input soliton pulse propagates 6 m, its central wavelength redshifts to a shift value of $\Delta_\lambda = 28$ nm and presents a quality factor of ≈ 0.8. This work shows that in both phenomena SPC and SSFS, not only is important to have either a high compression factor or a large displacement of the output soliton pulse, respectively, but also a high quality of the output pulse is. For the SPC it is desirable that the compressed pulse has the minimum pedestal energy, which implies a high quality factor. On the other hand, in the case of the SSFS phenomenon, a high pulse quality results in that most of the energy of the input soliton pulse is transferred to the shifted output soliton pulse. Therefore, an analysis of the pulse quality during the propagation of soliton pulses along HC-PBGFs is necessary in order to find an appropriate fiber structure as well as the input soliton pulse that promotes both SPC and SSFS.

5 Conclusions

In summary, a numerical investigation was mainly performed on soliton pulse compression and soliton self-frequency shift in hollow-core photonic bandgap fibers, at wavelengths of 800 nm and 1060 nm. The effects of both reducing the cross section size of the fiber structures and the input soliton order on such non linear phenomena has been studied. A pulse quality analysis has been introduced during the evolution of soliton pulses. In order to modelate the HC-PBGF structures, the commercial software Comsol was used. The generalized non linear Schrödinger equation was used in order to model the propagation of light pulses along the fiber.

In the first case, the influence of tuning the cross section size of a seven-cell hollow-core photonic bandgap fiber on both the pulse shape quality and the compression factor for unchirped pulses of 500 fs and at the wavelength of 800 nm was numerically studied. It was found that a tuning of the cross section size of the fiber with a tapering factor of 4.5% improves both features. The numerical results indicate a maximum compressed pulse with a compression factor of 5.7 with a temporal FWHM of 153.8 fs. The pulse reaches a peak power of 1.5851 MW with 77% of pulse shape quality. The length fiber at which the compressed pulse is reached is of 31 cm. The predicted compression factor is 3 times larger than that experimentally obtained in such propagation length of the pulse in a hollow-core photonic bandgap

fiber. Here, the results show that, with an appropriate tuning of the cross section size of a hollow-core photonic bandgap fiber, pulse compression can be improved significantly.

In the second case, a numerical investigation of low-order soliton evolution in a proposed seven-cell hollow-core photonic bandgap fiber is reported. In the numerical simulation, the pulse quality evolution in soliton pulse compression and soliton self-frequency shift in three fiber structures with different cross section sizes was investigated. In the simulation, unchirped soliton pulses (of 400 fs) at the wavelength of 1060 nm were considered. The results showed that the seven-cell HC-PBGFs, with a cross section size reduction of 2%, presents larger anomalous values of the second-order dispersion and greater values of the non linear parameter. If an input soliton pulse with order of $N = 3$ (which corresponds to an energy of 1.69 μJ) propagates a distance of 12 cm, it gets compressed with a compression factor of 5.6 and quality factor of 0.73. Meanwhile, after the input soliton pulse propagates 6 m, its central wavelength redshifts to a shift value of $\Delta_\lambda = 28$ nm and presents a quality factor of ≈ 0.8. This work shows that in both phenomena SPC and SSFS not only is important to have either a high compression factor or a large displacement of the output soliton pulse, respectively, but also a high quality of the output pulse is. For the SPC it is desirable that the compressed pulse has the minimum pedestal energy, which implies a high quality factor. On the other hand, in the case of the SSFS phenomenon, a high pulse quality results in that most of the energy of the input soliton pulse is transferred to the shifted output soliton pulse. Therefore, an analysis of the pulse quality during the propagation of soliton pulses along HC-PBGFs is necessary in order to find an appropriate fiber structure as well as the input soliton pulse that promotes both SPC and SSFS.

From the results, it can be inferred that an appropriate tuning of the HC-PBGF

structure can promote one or another non linear phenomena. However, the required fine tuning can be a practical limitation.

I belive the work can have practical applications and the results will certainly be useful from the point of view of engineering of photonic crystal fibers and optimizing their performance for pulse compression and soliton self-frequency shift. I hope that the results shown here will motivate the experimental investigation in this new and important technology.

A Papers, conferences and workshops

Published papers

- N. González-Baquedano, I. Torres-Gómez, N. Arzate, A. Ferrando and, D. E. Ceballos-Herrera, *"Pulse quality analysis on soliton pulse compression and soliton self-frequency shift in a hollow-core photonic bandgap fiber,"* Optics Express **21,** 9132–9143 (2013).

- N. González-Baquedano, N. Arzate, I. Torres-Gómez, A. Ferrando, D. E. Ceballos-Herrera, and C. Milián, *"Femtosecond pulse compression in a hollow-core photonic bandgap fiber by tuning its cross section,"* Photonics and Nanostructures – Fundamentals and Applications **10,** 594–601 (2012).

- A. Ferrando, C. Milián, D. Ceballos, N. González, I. Orquín, M. A. García-March, M. Zacarés, Ll. Monreal, J. M. Isidro, and P. Fernández de Córdoba, *"Modeling nonlinear waves in photonics, plasmonics and cold atoms,"* Óptica pura y aplicada **44,** 455–461 (2011).

- N. González Baquedano, S. Vargas, N. Arzate, I. Torres-Gómez, A. Martínez-Ríos, D. E. Ceballos-Herrera, A. Ferrando, and C. Milián, *"Modeling the tapering effects on the modal parameters of a hollow-core photonic bandgap fiber,"* in *Eight Symposium Optics in Industry,* E. Rosas, N. Arzate, I. Torres and J.

Sumaya, eds., Proc. SPIE **8287,** 828701 (2011).

- A. Ferrando, C. Milián, N. González, G. Moltó, P. Loza, M. Arevalillo-Herráez, M. Zacarés, I. Torres-Gómez, V. Hernández, *"Desingning supercontinuum spectra usig Grid technology*," in *2nd Workshop on Specialty Optical Fibers and Their Applications,* J. Hernández-Cordero, I. Torres-Gómez, and A. Méndez, eds., Proc. SPIE **7839,** 78390W (2010).

Conferences and workshops

- N. González-Baquedano, N. Arzate, I. Torres-Gómez, A. Ferrando, D. E. Ceballos-Herrera, and C. Milián, *"Femtosecond pulse compression in a hollow-core photonic bandgap fiber by tuning its cross section*," in *Mexican Optics and Photonic Meeting,* San Luis Potosí, México (2012).

- N. González Baquedano, S. Vargas, N. Arzate, I. Torres-Gómez, A. Martínez-Ríos, D. E. Ceballos-Herrera, A. Ferrando, and C. Milián, *"Soliton compression in a tapered hollow-core photonic bandgap fiber*," in *ICO-22,* Puebla, México (2011).

- C. Milián, N. González-Baquedano, D. Ceballos, A. Ferrando, *"Optimization of supercontinuum spectrum in PCF*," Oral presentation, I Valencian Workshop on computational photonics, Valencia, Spain (2010).

- N. González-Baquedano, N. Arzate, I. Torres-Gómez, *"Estudio de las fibras de cristal fotónico para la generación de segundo armónico*," in *IX Escuela de Óptica Moderna,* Puebla, México (2009).

References

[1] F. Benabid and P. J. Roberts, *Linear and nonlinear optical properties of hollow core photonic crystal fiber*, J. Mod. Opt. **58**, 87 (2011).

[2] P. Russell, *Photonic crystal fibers*, Science. **299**(5605), 358 (2003).

[3] T. A. Birks, P. J. Roberts, P. S. J Russell, D. M Atkin, and T. J Shepherd, *Full 2-d photonic bandgaps in silica-air structures*, Electronic Letters **31**(13), 1941 (1995).

[4] R. F. Cregan, B. J. Mangan, J. C. Knight, T. A. Birks, P. St. J. Russell, P. J. Roberts, and D. C. Allan, *Single-mode photonic band gap guidance of light in air*, Science. **285**(13), 1537 (1999).

[5] F. Couny, F. Benabid, and P. S. Light, *Large-pitch kagome-structured hollow-core photonic crystal fiber*, Opt. Lett. **31**(24), 3574 (2006).

[6] R. Amezcua-Correa, N. G. R. Broderick, M. F. Poletti, and D. J. Richardson, *Design of 7 and 19 cells core air-guiding photonic crystal fibers for low-loss, wide bandwidth and dispersion controlled operation*, Optics Express **15**(26), 17577 (2007).

[7] R. Amezcua-Correa, F. Gérôme, S. G. Leon-Saval, N. G. R. Broderick, T. A. Birks, and J. C. Knight, *Control of surface modes in low loss hollow-core photonic bandgap fibers*, Optics Express **16**(2), 1142 (2008).

[8] Z. Várallyay, K. Saitoh, J. Fekete, K. Kakihara, M. Koshiba, and R. Szipocs, *Reversed dispersion slope photonic bandgap fibers for broadband dispersion control in femtosecond fiber lasers*, Optics Express **16**(20), 15603 (2008).

[9] F. Couny, P. J. Roberts, T. A. Birks, and F. Benabid, *Square-lattice large-pitch hollow-core photonic crystal fiber*, Optics Express **16**(25), 20626 (2008).

[10] H. K. Kim, M. J. F Digonnet, and G.S. Kino, *Air-core photonic-bandgap fiber-optic gyroscope*, J. of Lightwave Technol. **24**, 3169 (2006).

[11] S. Blin, H. K. Kim, M. J. F. Digonnet, and G. S. Kino, *Reduced thermal sensitivity of a fiber-optic gyroscope using an air-core photonic-bandgap fiber*, J. of Lightwave Technol. **25**, 861 (2007).

[12] A. Hongo, K. Morosawa, K. Matsumoto, T. Shiota, and T. Hashimoto, *Transmission of kilowatt-class CO_2 laser light through dielectric-coated metallic hollow waveguides for material processing*, Appl. Opt. **31**, 5114 (1992).

[13] R. K. Nubling and J. A. Harrington, *Hollow-waveguide delivery systems for high-power, industrial CO_2 lasers*, Appl. Opt. **34**(3), 372 (1996).

[14] B. Dekel, A. Inberg, N. Croitoru, S. Shalem, and A. Katzir, *Hollow glass waveguides and silver halide fibers as scanning elements for CO_2 laser marking systems*, Optical Engineering **39**, 1384 (2000).

[15] A. F. Kosolapov, A. D. Pryamikov, A. S. Biriukov, V. S. Shiryaev, M. S. Astapovich, G. E. Snopatin, V. G. Plotnichenko, M. F. Churbanov, and E. M. Dianov, *Demonstration of CO_2-laser power delivery through chalcogenide-glass fiber with negative-curvature hollow core*, Optics Express **19**(25), 25723 (2011).

[16] S. H. Aref, R. Amezcua-Correa, J. P. Carvalho, O. Frazão, P. Caldas, J. L. Santos, F. M. Arajo, H. Latifi, F. Farahi, L. A. Ferreira, and J. C. Knight,

Modal interferometer based on hollow-core photonic crystal fiber for strain and temperature measurement, Optics Express **17**(21), 18669 (2009).

[17] S. D. Lim, K. Ma, J. H. Jeong, G. Kim, K. Lee, J.-M. Jeong, and S. B. Lee, *In situ gas sensing using a remotely detectable probe with replaceable insert*, Optics Express **20**(2), 1727 (2012).

[18] S. H. Aref, R. Amezcua-Correa, J. P. Carvalho, O. Frazão, J. L. Santos, F. M. Araújo, H. Latifi, F. Farahi, L. A. Ferreira, and J. C. Knight, *Spectral characterization of a photonic bandgap fiber for sensing applications*, Appl. Opt. **49**(10), 1870 (2010).

[19] W. Jin, H. F. Xuan, and H. L. Ho, *Sensing with hollow-core photonic bandgap fibers*, Meas. Sci. Technol. **21**(094014) (2010).

[20] Y. Zhao, R. Lv, Y. Ying, and Q. Wang, *Hollow-core photonic crystal fiber fabryperot sensor for magnetic field measurement based on magnetic fluid*, Optics & Laser Technology **44**, 899 (2012).

[21] P. Ghenuche, H. Rigneault, and J. Wenger, *Hollow-core photonic crystal fiber probe for remote fluorescence sensing with single molecule sensitivity*, Optics Express **20**(27), 28379 (2012).

[22] H. Gong, C. C. Chan, Y. Zhang, W. Wong, and X. Dong, *Temperature sensor based on modal interference in hollow-core photonic bandgap fiber with collapse splicing*, IEEE Sensors Journal **12**(5), 1421 (2012).

[23] A. Khetani, V. S. Tiwari, A. Harb, and H. Anis, *Monitoring of heparin concentration in serum by Raman spectroscopy within hollow core photonic crystal fiber*, Optics Express **19**(16), 15244 (2011).

[24] S. O. Konorov, A. B. Fedotov, O. A. Kolevatova, V. I. Beloglazov, N. B. Skibina, A. V. Shcherbakov, E. Wintner, and A. M. Zheltikov, *Laser breakdown with millijoule trains of picosecond pulses transmitted through a hollow-core photonic-crystal fibre*, J. Phys. D: Appl. Phys. **36**(12), 1375 (2003).

[25] J. Shephard, J. Jones, D. Hand, G. Bouwmans, J. Knight, P. Russell, and B. Mangan, *High energy nanosecond laser pulses delivered single-mode through hollow-core PBG fibers*, Optics Express **12**(4), 717 (2004).

[26] S. O. Konorov, V. P. Mitrokhin, A. B. Fedotov, D. A. Sidorov-Biryukov, V. I. Beloglazov, N. B. Skibina, A. V. Shcherbakov, E. Wintner, M. Scalora, and A. M. Zheltikov, *Laser ablation of dental tissues with picosecond pulses of 1.06-μm radiation transmitted through a hollow-core photonic-crystal fiber*, Appl. Opt. **43**(11), 2251 (2004).

[27] S. O. Konorov, V. P. Mitrokhin, A. B. Fedotov, D. A. Sidorov-Biryukov, V. I. Beloglazov, N. B. Skibina, E. Wintner, M. Scalora, and A. M. Zheltikov, *Hollow-core photonic-crystal fibres for laser dentistry*, Physics in Medicine and Biology **49**(7), 1359 (2004).

[28] B. A. Flusberg, J. C. Jung, E. D. Cocker, E. P. Anderson, and M. J. Schnitzer, *In vivo brain imaging using a portable 3.9 gram two-photon fluorescence microendoscope*, Optics Lett. **30**(17), 2272 (2005).

[29] F. Benabid, F. Couny, J. C. Knight, T. A. Birks, and P. S. J. Russell, *Compact, stable and efficient all-fibre gas cells using hollow-core photonic crystal fibres*, Nature. **434**, 488 (2005).

[30] J. C. Travers, W. Chang, J. Nold, N. Y. Joly, and P. St. J. Russell, *Ultrafast nonlinear optics in gas-filled hollow-core photonic crystal fibers*, J. Opt. Soc. Am. B **28**(12), A11 (2011).

[31] A. R. Bhagwat and A. L. Gaeta, *Nonlinear optics in hollow-core photonic bandgap fibers*, Optics Express **16**, 5035 (2008).

[32] F. Benabid, J. C. Knight, G. Antonopoulous, and P. S. J. Russell, *Stimulated Raman scattering in hydrogen-filled hollow-core photonic crystal fiber*, Science. **298**, 399 (2002).

[33] D. G. Ouzounov, F. R. Ahmad, D. Müller, N. Venkataraman, M. T. Gallagher, M. G. Thomas, J. Silcox, K. W. Koch, and A. L. Gaeta, *Generation of megawatt optical solitons in hollow-core photonic band-gap fibers*, Science. **301**, 1702 (2003).

[34] F. Benabid, G. Bouwmans, J. C. Knight, P. S. J. Russell, and F. Couny, *Ultra-high efficiency laser wavelength conversion in gas-filled hollow core photonic crystal fiber by pure stimulated rotational Raman scattering in molecular hydrogen*, Phys. Rev. Lett. **93**, 1195 (2004).

[35] F. Benabid, G. Antonopoulos, J. C. Knight, and P. S. J. Russell, *Stokes amplification regimes in quasi-CW pumped hydrogen-filled hollow-core photonic crystal fiber*, Phys. Rev. Lett. **95**, 213903 (2005).

[36] A. Abdolvand, A. Nazarkin, A. V. Chugreev, C. F. Kaminski, and P. St. J. Russell, *Solitary pulse generation by backward Raman scattering in H_2-filled photonic crystal fibers*, Phys. Rev. Lett. **103**, 183902 (2009).

[37] A. Nazarkin, A. Abdolvand, A. V. Chugreev, and P. St. J. Russell, *Direct observation of self-similarity in evolution of transient stimulated Raman scattering in gas-filled photonic crystal fibers*, Phys. Rev. Lett. **105**, 173902 (2010).

[38] P. Londero, V. Venkataraman, A. R. Bhagwat, A. D. Slepkov, and A. L. Gaeta, *Ultralow-power four-wave mixing with Rb in a hollow-core photonic band-gap fiber*, Phys. Rev. Lett. **103**, 043602 (2009).

[39] F. Benabid, P. S. Light, F. Couny, and P. S. J. Russell, *Electromagnetically-induced transparency grid in acetylene-filled hollow-core PCF*, Optics Express **13**, 5694 (2005).

[40] S. Ghosh, J. Sharping, D. G. Ouzounov, and A. L. Gaeta, *Resonant optical interactions with molecules confined in photonic band-gap fibers*, Phys. Rev. Lett. **94** (2005).

[41] F. Benabid, J. C. Knight, and P. S. J. Russell, *Particle levitation and guidance in hollow-core photonic crystal fiber*, Optics Express **10**(21), 1195 (2002).

[42] J. C. Knight, *Photonic crystal fibres*, Nature **386**, 143 (1997).

[43] D. G. Ouzounov, C. J. Hensley, A. L. Gaeta, N. Venkataraman, M. T. Gallagher, and K. W. Koch, *Soliton pulse compression in photonic band-gap fibers*, Optics Express **13**, 6153 (2005).

[44] F. Gérôme, K. Cook, A. K. George, W. Wadsworth, and J. C. Knight, *Delivery of sub-100fs pulses through 8m of hollow-core fiber using soliton compression*, Optics Express **15**, 7126 (2007).

[45] Y. Meng, S. Zhang, C. Jin, H. Li, and X. Wang, *Enhanced compression of femtosecond pulse in hollow-core photonic band gap fibers*, Optics Communications **283**, 2411 (2010).

[46] F. Luan, J. C. Knight, P. S. J. Russell, S. Campbell, D. Xiao, D. T. Reid, B. J. Mangan, D. P. Williams, and P. J. Roberts, *Femtosecond soliton pulse delivery*

at 800 nm wavelength in hollow-core photonic bandgap fibers, Optics Express **12**, 835 (2004).

[47] D. V. Skryabin, *Coupled core-surface solitons in photonics crystal fibers*, Optics Express **12**, 4841 (2004).

[48] J. C. Knight, F. Gérôme, and W. J. Wadsworth, *Hollow-core photonic crystal fibres for delivery and compression of ultrashort optical pulses*, IEEE J. Quantum Electron. **39**, 1047 (2007).

[49] J. Lægsgaard and P. J. Roberts, *Dispersive pulse compression in hollow-core photonic band gap fibers*, Optics Express **16**, 9268 (2008).

[50] J. Lægsgaard, *Soliton formation in hollow-core photonic bandgap fibers*, Appl. Phys. B **95**, 2093 (2009).

[51] M. G. Welch, K. Cook, R. Amezcua-Correa, F. Gérôme, W. J. Wadsworth, A. V. Gorbach, D. V. Skryabin, and J. C. Knight, *Solitons in hollow core photonic crystal fiber: Engineering nonlinearity and compressing pulses*, J. of Lightwave Technol. **27**, 1644 (2009).

[52] A. V Gorbach and D. V Skryabin, *Soliton self-frequency shift, non-solitonic radiation and self-induced transparency in air-core fibers*, Optics Express **16**, 4858 (2008).

[53] O. H. Heckl, C. J. Saraceno, C. R. E. Baer, T. Südmeyer, Y. Y. Wang, Y. Cheng, F. Benabid, and U. Keller, *Temporal pulse compression in a xenon-filled kagome-type hollow-core photonic crystal fiber at high average power*, Optics Express **19**(20), 19142 (2011).

[54] A. A. Ivanov, A. A. Podshivalov, and A. M. Zheltikov, *Frequency-shifted megawatt soliton output of a hollow photonic-crystal fiber for time-resolved coherent anti-Stokes Raman scattering microspectroscopy*, Optics Lett. **31**, 3318 (2006).

[55] B-W. Liu, M-L. Hu, X-H. Fang, Y-F. Li, L. Chai, C-Y. Wan, W. Tong, J. Luo, A. A. Voronin, and A. M. Zheltikov, *Stabilized soliton self-frequency shift and 0.1-PHz sideband generation in a photonic-crystal fiber with an air-hole-modified core*, Optics Express **16**, 14987 (2008).

[56] F. Gérôme, P. Dupriez, J. Clowes, J. C. Knight, and W. J Wadsworth, *High power tunable femtosecond soliton source using hollow-core photonic bandgap fiber, and its use for frequency doubling*, Optics Express **16**, 2381 (2008).

[57] N. González-Baquedano, N. Arzate, I. Torres-Gómez, A. Ferrando, D. E. Ceballos-Herrera, and C. Milián, *Femtosecond pulse compression in a hollow-core photonic bandgap fiber by tuning its cross section*, Photonics and Nanostructures - Fundamentals and Applications **10**, 594 (2012).

[58] R. Amezcua-Correa, *Development of hollow-core photonic bandgap fibres free of surfaces modes*, Ph.D. thesis, University of Southampton (2009).

[59] A. Bjarklev, J. Broeng, and A. S. Bjarklev, *Photonic Crystal Fibres* (Springer, 2003), 1st ed.

[60] K. Saitoh, *Numerical modeling of photonic crystal fibers*, J. of Lightwave Technol. **23**(11), 3580 (2005).

[61] J. D. Joannopoulos, S. G. Johnson, J. N. Winn, and R. D. Meade, *Photonic crystals. Molding the flow of light* (Princeton Univ. Press, 2008), 2nd ed.

[62] J. M. Dudley and J. R. Taylor, *Ten years of nonlinear optics in photonic crystal fibre*, Nature Photonics **3**, 85 (2009).

[63] T. A. Birks and W. Y. Li, *The shape of fiber tapers*, J. of Lightwave Technol. **10**, 432 (1992).

[64] A. Ferrando, *Designing the properties of dispersion-flattened photonic crystal fibers*, Optics Express **9**(13), 687 (2001).

[65] C. J. Hensley, D. G. Ouzounov, and A. L. Gaeta, *Silica-glass contribution to the effective non-linearity of hollow-core photonic band-gap fibers*, Optics Express **15**, 3507 (2007).

[66] J. Lægsgaard, et al., *Material effects in air-guiding photonic band gap fibers*, J. Opt. Soc. Am. B **20**, 2046 (2003).

[67] F. Poli, A. Cucinotta, and S. Selleri, *Photonic Crystal Fibers* (Springer, 2007).

[68] R. Amezcua-Correa, N. G. Broderick, M. N. Petrovich, F. Poletti, and D. J. Richardson, *Optimizing the usable bandwidth and loss through core design in realistic hollow-core photonic bandgap fibers*, Optics Express **14**, 7974 (2006).

[69] G. P. Agrawal, *Non-linear Fiber Optics* (Academic Press Inc., 2001), 3rd ed.

[70] J. Lægsgaard, N. A. Mortensen, and A. Bjarklev, *Mode areas and field-energy distribution in honeycomb photonic bandgap fibers*, J. Opt. Soc. Am. B **20**, 2037 (2003).

[71] G. P. Agrawal, *Applications of Nonlinear Fiber Optics* (Academic Press Inc., 2001).

[72] L. F. Mollenauer and J. P. Gordon, *Solitons in Optical Fibers* (Academic Press Inc., 2006).

[73] Y. S. Kivshar and G. P. Agrawal, *Optical Solitons* (Academic Press, 2003), 1st ed.

[74] E. M. Dianov, Z. S. Nikonova, A. M. Prokhorov, and V. N. Serkin, *Optimal compression of multi-soliton pulses in optical fibers*, Sov. Tech. Phys. Lett. **12**, 311 (1986).

[75] M. Y. Chen, H. Subbaraman, and R. T. Chen, *One stage pulse compression at 1554nm through highly anomalous dispersive photonic crystal fiber*, Optics Express **19**(22), 21809 (2011).

[76] K-T. Chan and W-H. Cao, *Enhanced compression of fundamentals solitons in dispersion decreasing fibers due to the combined effects of negative third-order dispersion and Raman self-scattering*, Optics Communications **184**, 463 (2000).

[77] N. González Baquedano, S. Vargas, N. Arzate, I. Torres-Gómez, A. Martínez-Ríos, D. E. Ceballos-Herrera, A. Ferrando, and C. Milián, *Modeling the tapering effects on the modal parameters of a hollow-core photonic bandgap fiber*, Proc. SPIE **8287**, 828701 (2011).

[78] J. M. Dudley, G. Genty, and S. Coen, *Supercontinuum generation in photonic crystal fiber*, Rev. Mod. Phys. **78**, 1135 (2006).